FM-CW LASER RADAR AT 10.6 MICRONS

Thomas Henry Chance

Library
Naval Postgraduate School
Monterey, California 93940

NAVAL POSTGRADUATE SCHOOL
Monterey, California

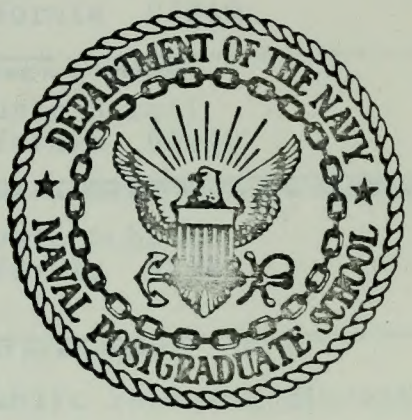

THESIS

FM-CW LASER RADAR AT 10.6 MICRONS

by

Thomas Henry Chance

December 1974

Thesis Advisor: C. H. Rothauge

Approved for public release; distribution unlimited.

T164026

UNCLASSIFIED

SECURITY CLASSIFICATION OF THIS PAGE (When Data Entered)

REPORT DOCUMENTATION PAGE		READ INSTRUCTIONS BEFORE COMPLETING FORM
1. REPORT NUMBER	2. GOVT ACCESSION NO.	3. RECIPIENT'S CATALOG NUMBER
4. TITLE (and Subtitle) FM-CW Laser Radar at 10.6 Microns		5. TYPE OF REPORT & PERIOD COVERED Electrical Engineer; December 1974 6. PERFORMING ORG. REPORT NUMBER
7. AUTHOR(s) Thomas Henry Chance		8. CONTRACT OR GRANT NUMBER(s)
9. PERFORMING ORGANIZATION NAME AND ADDRESS Naval Postgraduate School Monterey, California 93940		10. PROGRAM ELEMENT, PROJECT, TASK AREA & WORK UNIT NUMBERS
11. CONTROLLING OFFICE NAME AND ADDRESS Naval Postgraduate School Monterey, California 93940		12. REPORT DATE December 1974 13. NUMBER OF PAGES 117
14. MONITORING AGENCY NAME & ADDRESS(if different from Controlling Office) Naval Postgraduate School Monterey, California 93940		15. SECURITY CLASS. (of this report) Unclassified 15a. DECLASSIFICATION/DOWNGRADING SCHEDULE

16. DISTRIBUTION STATEMENT (of this Report)

Approved for public release; distribution unlimited

17. DISTRIBUTION STATEMENT (of the abstract entered in Block 20, if different from Report)

18. SUPPLEMENTARY NOTES

19. KEY WORDS (Continue on reverse side if necessary and identify by block number)

Optical Radar
Lidar
Optical Coherent Detection
Laser Radar
FM-CW Optical Radar

20. ABSTRACT (Continue on reverse side if necessary and identify by block number)

The feasibility of a continuous-wave frequency-modulated radar with a CO_2 laser as a transmitting source was investigated.

A developmental system was constructed and tested and the feasibility of an optical radar utilizing coherent detection at 10.6 microns was demonstrated. The radar had

DD FORM 1 JAN 73 1473 (Page 1) EDITION OF 1 NOV 65 IS OBSOLETE S/N 0102-014-6601

UNCLASSIFIED

SECURITY CLASSIFICATION OF THIS PAGE (When Data Entered)

Block #20 Continued

the capability of instantaneous range and velocity determination.

FM-CW Laser Radar at 10.6 Microns

by

Thomas Henry Chance
Lieutenant, United States Navy
BSEE, Purdue University, 1969
MSEE, Naval Postgraduate School, 1974

Submitted in partial fulfillment of the
requirements for the degree of

ELECTRICAL ENGINEER

from the

NAVAL POSTGRADUATE SCHOOL
December 1974

Thesis
C367
c.1

Library
Naval Postgraduate
Monterey, California

ABSTRACT

The feasibility of a continuous-wave frequency-modulated radar with a CO_2 laser as a transmitting source was investigated.

A developmental system was constructed and tested and the feasibility of an optical radar utilizing coherent detection at 10.6 microns was demonstrated. The radar had the capability of instantaneous range and velocity determination.

TABLE OF CONTENTS

LIST OF TABLES

LIST OF FIGURES

Figure

ACKNOWLEDGEMENTS

I desire to give recognition and express gratitude for the support given by the Naval Electronic Laboratory Center San Diego, Code 2500, particularly to Dr. Greg Mooradian and Rudy Krautwald. Also I am grateful for the assistance of Professors John Powers, T. F. Tao and C. H. Rothauge and for the technical support provided by Ross Seeley and Bob Moeller, all of the Naval Postgraduate School.

This research project was conducted with Lieutenant Maurice F. Fraunfelder, Jr., a fellow student at the Naval Postgraduate School.

Rockwell International Science Center provided a PbSnTe heterojunction p-i-n diode, courtesy of Dr. J. Longo, similar to the detector loaned by NELC (which was also manufactured by Rockwell International Science Center). This detector had a slightly higher quantum efficiency than the one provided by NELC but did not have as high a frequency response even when back biased at .6 v. It was operated at 28-35 MHz (vice 35-45 MHz) but the frequency limitation still reduced the output to 5 db below that of the detector utilized in the system.

Aerojet Electrosystems Co. also provided a PbSnTe heterojunction p-n diode, courtesy of Dr. Peter Wang, but although it had a good quantum efficiency, its frequency response was much too low to be utilized in the system.

I. INTRODUCTION

A continuous-wave frequency-modulated radar provides a means of determining both range and relative velocity of a target. Since the radar is continuous-wave rather than pulsed, it enables realization of a given range capability without requiring high peak power capability such as would be required by a pulse radar. FM-CW radars have been developed for years but with the advent of the laser, a transmit power source of extremely high frequency and coherence became available.

Initially there was not the laser stability nor the means of frequency modulation of the beam available to make a system such as this practical. This capability exists now and was utilized in the developmental system.

The laser source provides a narrow beam and enables the use of a high-gain optical antenna which is small and lightweight (since gain is proportional to λ^{-2} and λ is 10.6 μm). This narrow beam allows excellent bearing resolution but requires a relatively long search time for any given volume of interest. It would also require excellent beam steering capability for a tracking application.

Heterodyne detection of 10.6 μm radiation at high IF frequency has only recently become feasible with the development of fast detectors with a cut-off wavelength greater than 10.6 μm. Heterodyning also provides higher sensitivity and low vulnerability to jamming.

Operation at 10.6 μm wavelength is outside the capability of any known intercept receiver and could not be detected by any known anti-radiation seeker.

II. GENERAL SYSTEM CONSIDERATIONS

A. FM-CW

FM-CW radars offer several distinct advantages over standard pulse radars. In the CW radar the ratio of peak power to average power is near or equal to one. Since the maximum range of a radar is proportional to the fourth root of the average power this allows for good range capability without requiring components and circuitry capable of providing and switching high power and voltages as in a pulse radar [1]. Elimination of this requirement results in large savings in system size and expense.

$$R_{max} = \left(\frac{P_t G \sigma A_e}{16\pi^2 P_{min}}\right)^{\frac{1}{4}} \qquad (1)$$

where P_t is the average transmitted power, G is the antenna gain, σ is the target cross section, A_e is the effective receive aperture and P_{min} is the minimum required return signal power [2]. Normal FM-CW radars utilize two antennas and require feed over cancellation [3] while pulse radars require one antenna and a duplexer. Both these approaches are improved on by an optical radar which can use one antenna with no cancellation or duplexing. Additionally an optical antenna provides extremely high gain with small size.

1. Analysis of a FM-CW Radar System Using Triangular Modulation

FM-CW radars determine range and velocity by analyzing the difference between the frequencies of the return

and transmitted signals. If the transmitted signal is as shown in Figure 1 where $F_{modulating} = T^{-1}$ is the modulating frequency and $F_{transmit}$ is the frequency of the transmitted signal, the return signal reflected from a stationary target will be identical to that being transmitted only delayed ΔT.

$$\Delta T = \frac{2R}{c} \tag{2}$$

where R is the target range and c is the free space velocity of the propagation of light. The time-frequency display of the transmit and return signals is shown in Figure 2.

If the instantaneous transmit and return signals are mixed the difference frequency can be extracted and processed. The time-frequency display of the difference frequency is shown in Figure 3.

The difference frequency directly yields range information. The rate of change of transmitted frequency (df/dt) is given by

$$\frac{df}{dt} = \frac{2\Delta F}{T/2} = 4\Delta F\ F_m \tag{3}$$

where T is the modulating period, $2\Delta F$ is the total range of frequency deviation and F_m is the modulating frequency.

Range frequency and thus range information is provided from

$$F_{range} = \frac{df}{dt} \cdot \Delta T, \tag{4}$$

$$R_{ange} = \frac{c \cdot \Delta T}{2} = \frac{c}{2} \cdot \frac{F_{range}}{df/dt} . \tag{5}$$

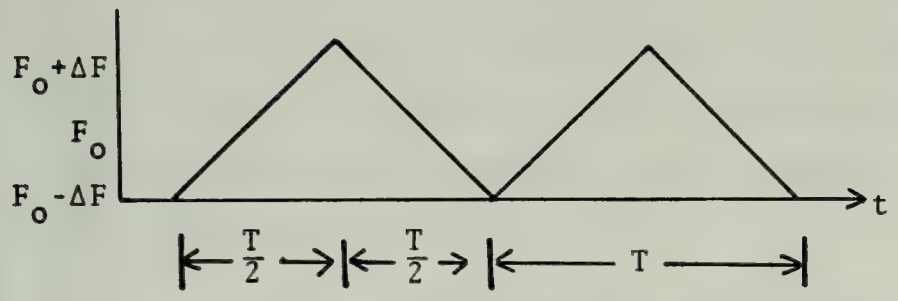

Figure 1. Frequency vs. Time of Transmit Signal.

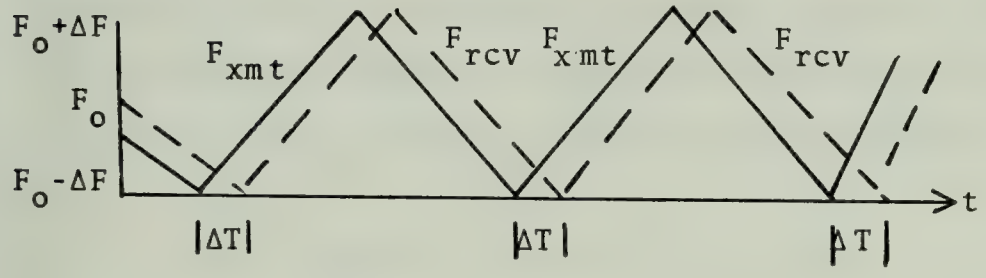

Figure 2. Transmit and Return Signals vs. Time.

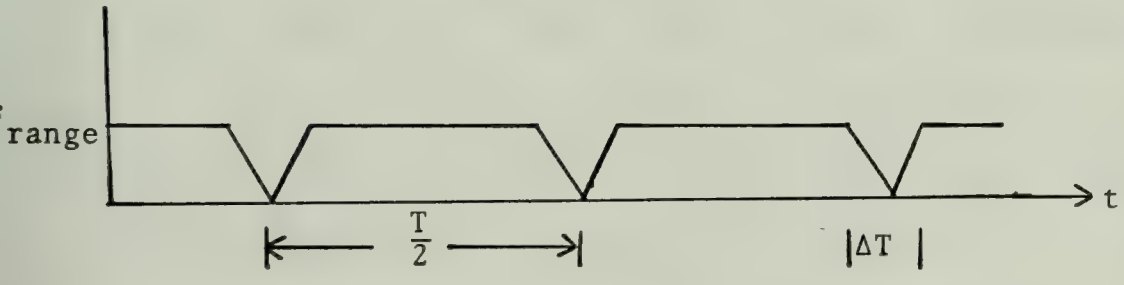

Figure 3. Range Frequency vs. Time.

Since for a given system df/dt is constant;

$$R_{ange} = \text{constant} \cdot F_{range} \tag{6}$$

and thus range can be directly determined from the transmit and return difference frequency.

If there is a relative velocity between the radar and target the returned signal will have an additional shift in frequency due to doppler shift. Doppler shift is given by the relationship [4]

$$F_{doppler} = \frac{2 \cdot V_{elocity} R_{elative} \cdot F_o}{c} \tag{7}$$

where F_o is the frequency of the transmitted optical signal. Comparison of the transmit and return signals, when the return signal has doppler information from the positive relative velocity, yields a time-frequency display as in Figure 4.

The difference frequencies F_a and F_b can be processed to extract both range and doppler frequency information.

$$F_{xmt} > F_{rcv} \quad F_a = |F_{xmt} - F_{rcv}| = F_{range} - F_{doppler} \tag{8}$$

$$F_{rcv} > F_{xmt} \quad F_b = |F_{xmt} - F_{rcv}| = F_{range} + F_{doppler} \tag{9}$$

In systems where the expected range frequency offset is greater than the expected doppler shift, range and doppler information can be extracted by processing as:

$$F_{range} = \frac{F_a + F_b}{2} = \frac{(F_{range} - F_{doppler}) + (F_{range} + F_{doppler})}{2} \tag{10}$$

$$F_{doppler} = \frac{F_b - F_a}{2} = \frac{(F_{range} + F_{doppler}) - (F_{range} - F_{doppler})}{2} \tag{11}$$

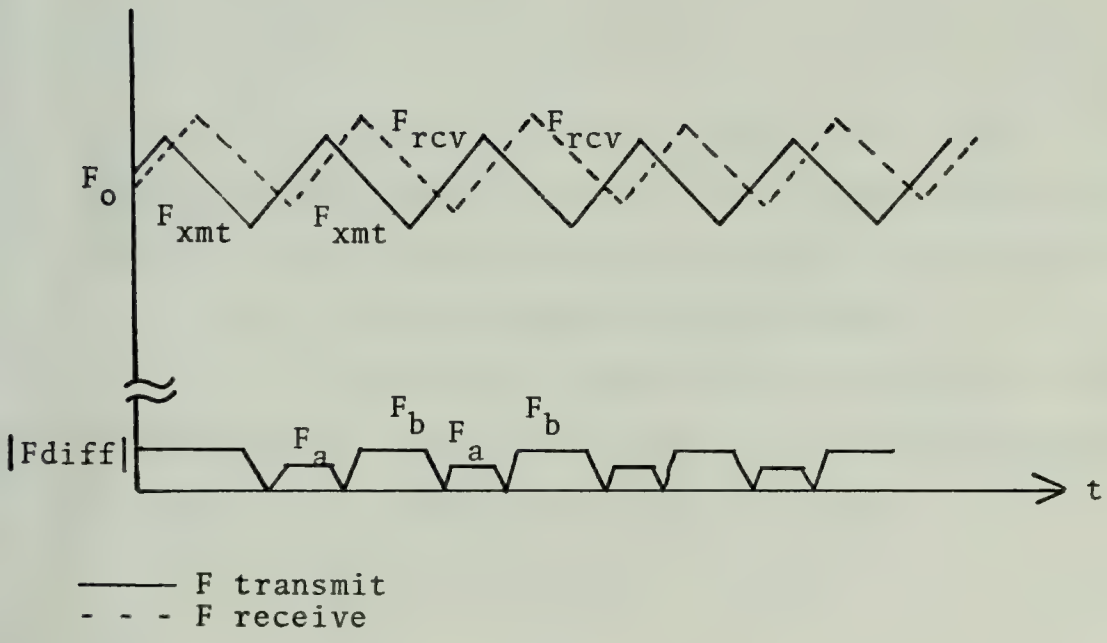

Figure 4. Return from Target with Positive Relative Velocity.

If the expected doppler frequency shift is greater than the expected range frequency of equations (10) and (11) are reversed.

It is readily seen from equation (7) that the relative velocity is the product of a constant times the doppler shift (any variation in F_o due to modulation is negligible).

2. Signal Processing in a FM-CW Radar

There are numerous interactions between bandwidth requirements, signal processing and expected target performance. The receiver input bandwidth must be great enough to accommodate the return signal which is both FM and possibly doppler shifted, IF bandwidth and processing filters must be able to process difference frequencies, doppler broadening and range broadening. These bandwidths affect range and velocity determination and available modulation rates.

a. Receiver Bandwidth Requirements

The receiver bandwidth must be able to pass the FM spectrum of the transmit signal and also accommodate any doppler shift within the range of interest.

The bandwidth requirement of an FM system is given by

$$BW \simeq 2(1+\beta)F_m = 2(1+\Delta F/F_m)F_m. \qquad (12)$$

For a frequency excursion of 5 MHz at a modulating rate of 1.75 kHz this yields a bandpass requirement of 10.0035 MHz or approximately 2 ΔF.

As stated, additional allowance must be made for doppler offset. The amount of the offset is given by

equation (7). For a CO_2 laser the optical frequency is 2.83×10^{13} Hz. This yields

$$F_{doppler} = \frac{2 \cdot V_{relative} \cdot F_o}{c} = 52.4 \text{ kHz/km/hr}$$

$$\simeq 95.8 \text{ kHz/knot.} \qquad (13)$$

If the maximum relative velocity of interest was 1000 knots this would require an allowable offset of ±95.8 MHz. This requirement for a wide receiver bandwidth yields a very wide noise bandwidth which reduces receiver sensitivity. This can be largely offset by narrower velocity range of interest.

b. Range Spectrum Analysis

The spectrum of the range frequency requires an IF bandwidth sufficient to pass the spectrum. Regretably the spectrum of the range frequency varies with the range. This spectrum will be considered at very short range and at a range of one half the maximum unambiguous range.

(1) Spectrum of a Near Range Target. Figures 5 and 6 show the frequency-time relationship for a near range target. The frequency spectrum of the range frequency can be closely approximated by assuming rectangular pulses of duration t and period ΔT. This spectrum is shown in Figure 7. It should be noted that the first sidebands exist in the main lobe at reduced magnitudes. As the range increases the ratio of the pulse width to the period decreases and the lobe spreads until at the point where the pulse width is less than half the period two sidebands will exist within the main lobe of the spectrum. Before this point is reached the approximation of a rectangular pulse is not nearly as

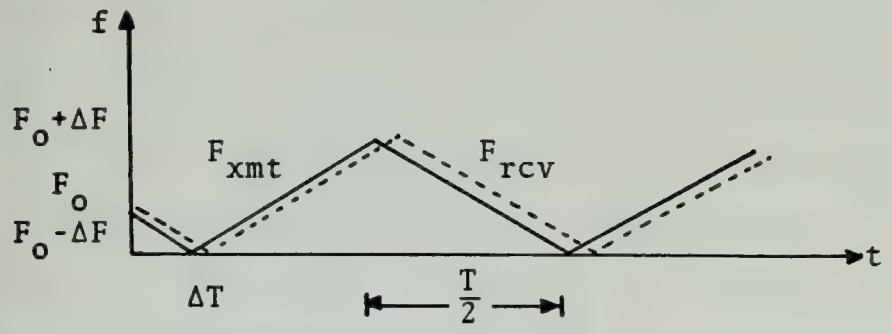

Figure 5. Frequency vs. Time Near Range Target.

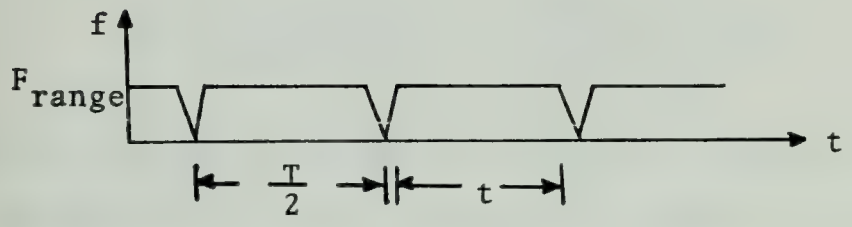

Figure 6. Range Frequency vs. Time Near Range Target.

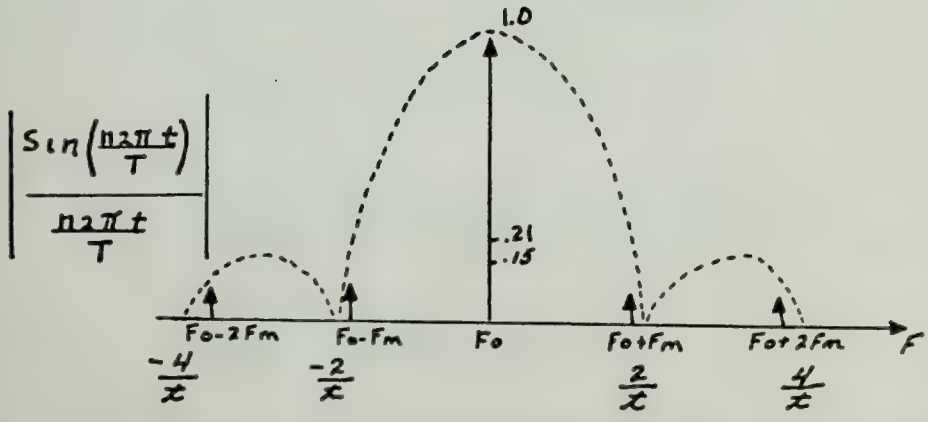

Figure 7. Frequency Spectrum of Range Frequency. $t=\frac{T}{2}$ $F_m=\frac{2}{T}$

exact and a better approximation is that of a trapezoidal pulse.

(2) Spectrum of a Far Range Target. Figures 8 and 9 show the frequency-time relationships for a target whose range is one half the maximum unambiguous range of the radar. The frequency spectrum of the range frequency is that of a trapezoidal pulse whose maximum frequency exists for one half the period. The spectrum envelope is found from the product of [5,6]

$$\frac{\sin(\pi n t_1/T/2)}{\pi n t_1/T/2} \cdot \frac{\sin[\pi n(t_1+t_o)/T/2]}{\pi n(t_1+t_o)/T/2} = \frac{\sin(\pi n t_1/T/2)}{\pi n t_1/T/2} \cdot \frac{\sin[\pi n 3 t_1/T/2]}{\pi n 3 t_1/T/2} \tag{14}$$

This spectrum is shown in Figure 10. It can be seen that the spectrum is being spread and a greater percentage of the signal energy is in the first sidebands.

c. Spectrum Spread Acceleration

An accelerating target causes a spread in the doppler frequency of the return signal. This is analyzed in a straightforward manner as follows:

$$F_{doppler} = \frac{2 \cdot V_{el} \cdot F_o}{c} \tag{7}$$

$$\frac{dF_d}{dt} = \frac{d}{dt}\left(\frac{2 \cdot V_{el} \cdot F_o}{c}\right) = \frac{2 \cdot F_o}{c} \cdot A_{ccel} \tag{15}$$

$$\Delta F_d = \frac{2 \cdot A_{ccel}}{\lambda_o} \cdot \Delta t \tag{16}$$

Δt is determined by the filter bandwidth so in the limit of the bandwidth

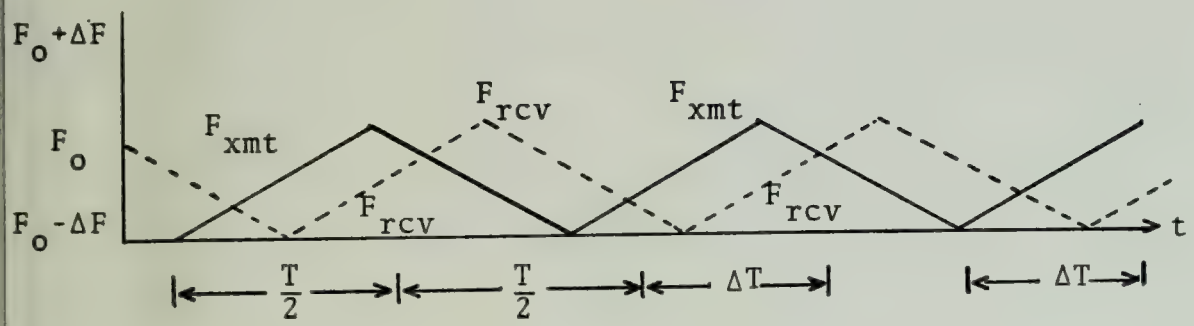

Figure 8. Frequency vs. Time Range = ½ Unambiguous Range.

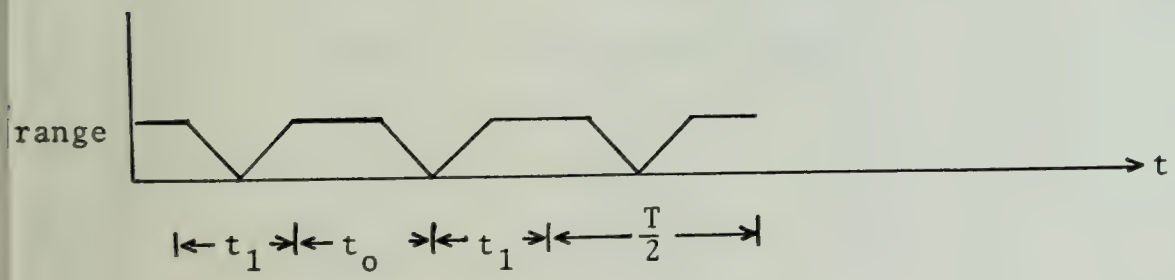

Figure 9. Range Frequency vs. Time Range = ½ Unambiguous Range.

$$\frac{\sin(2n\pi t_1/T)}{2n\pi t_1/T} \cdot \frac{\sin(6n\pi t_1/T)}{6n\pi t_1/T}$$

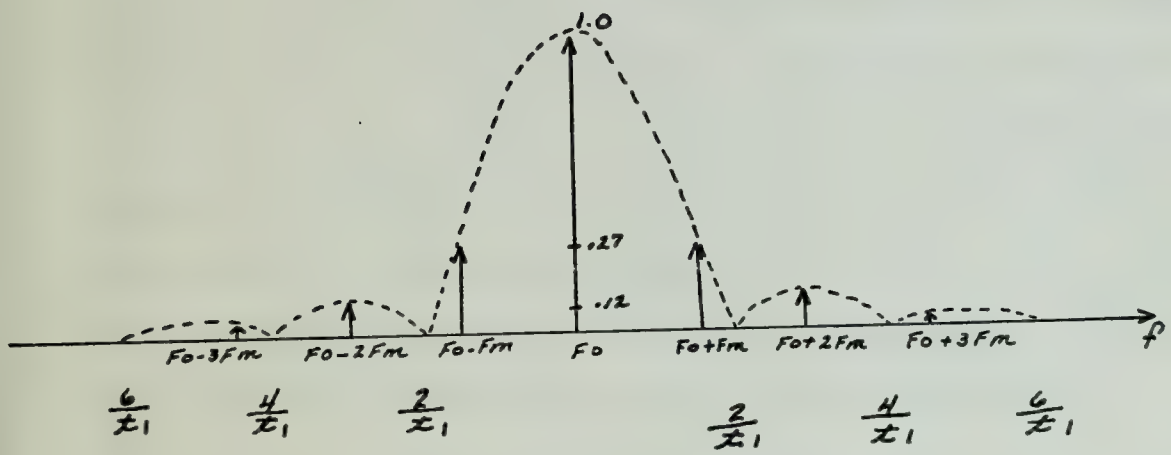

Range = ½ Unambiguous Range

$t_o = 2t_1$

$4t_1 = T/2 = 1/F_m$

Sidelobes 18.4 db down

Figure 10. Frequency Spectrum of Range Frequency.

$$\Delta t \simeq \frac{1}{BW} = \frac{1}{\Delta F} \tag{17}$$

$$\Delta F = \frac{2 \cdot A_{rel}}{\lambda_o} \tag{18}$$

where ΔF is the maximum allowable spreading of the spectrum. In practice the filter bandwidths are sufficient to accommodate very high accelerations.

d. Range Resolution

Range resolution is determined by the bandpass of the resolution filter or the spectrum width of the range frequency, whichever is greater. A well designed system will have a filter width whose response time corresponds to the modulating period and with the exception of targets approaching the maximum unambiguous range this will be sufficient for resolution calculations. The maximum unambiguous range can be determined by the following relationship

$$R_{unambiguous} = \frac{c}{2} \cdot \frac{T_{modulation}}{2} . \tag{19}$$

This limitation is determined by the propagation time for the target signal and the period of the modulating ramp. If the modulation rate is matched to the range filter (it can be slower) the range resolution is a direct function of the modulation bandwidth [6].

$$\Delta R = \frac{c}{2} \cdot \frac{\text{Filter BW}}{df/dt} . \tag{20}$$

From equation (2) and matching the filter to F_m this becomes [7]

$$\Delta R = \frac{c}{2} \cdot \frac{1}{2 \cdot \Delta F} \qquad (21)$$

which indicates that improved resolution requires a larger frequency excursion of the FM signal.

e. Velocity Resolution

Velocity resolution is similar to range resolution in that the wider the filter bandwidth the poorer the velocity resolution. Doppler resolution is given by the relationship

$$\Delta V_{el} = \frac{c \cdot \Delta F_{doppler}}{2F_o} = \frac{c \cdot \text{Filter BW}}{2F_o} \qquad (22)$$

f. Signal to Noise Effect of Collapsing the FM Return

When the transmit and received signals are mixed together the spectra of the two signals collapse and there results a relatively narrow frequency signal which is a function of target range and velocity. The resultant signals can be passed through bandpass filters and thus the resultant noise bandwidth is drastically reduced while the signal information is passed. The overall effect of this processing is to reduce the noise present and greatly improve the signal to noise ratio.

g. Range and Velocity Filtering

A means of determining the range or velocity frequencies is necessary in order to provide the inherent information. One method for doing this is to feed the information into a parallel bank of filters and provide a display according to which filter passes the information.

An alternate and more efficient approach is to utilize a sliding filter which sweeps the spectrum with respect to time in a known controlled manner. This approach allows relatively high resolution over a broad range with relatively few components and thus less bulk and expense.

B. MODULATION OF A LASER BEAM

1. Historical Basis of Acousto-Optic Modulation

The diffraction of light by accoustical waves in a medium was predicted by Brillouin in 1922 [9]. This phenomonon was observed by Debye and Sears in 1932 and is now known as the Debye-Sears effect. There was some initial investigation of the effect but until the advent of the laser to provide a high intensity beam which is highly coherent in both time and space no important application was seen and interest waned.

The mechanism by which acousto-optic modulation is accomplished is known as the photoelastic effect. This effect is the change in the index of refraction due to mechanical strain and is present in some crystals and liquids. Ultrasonic waves propagating through a material produce mechanical strains which in turn cause variations in the index of refraction. In this case the variation is known as the acousto-optic effect.

2. The Debye-Sears Effect

When a plane wave of light of angular frequency, ω, enters a slab of material with an index of refraction, n, the velocity of light in the material is reduced by the

factor n from its free space velocity c. The optical wavelength λ in the slab is

$$\lambda = \frac{2\pi c}{n\omega} \tag{23}$$

and the material acts as an optical delay line with a time delay t for a given length ℓ.

$$t = \frac{\ell n}{c} . \tag{24}$$

The delay, ϕ, corresponds to a phase delay of

$$\phi = \omega t = \frac{\omega \ell n}{c} . \tag{25}$$

Equation (25) can also be expressed as

$$\phi = \frac{2\pi f \ell n}{c} = \frac{2\pi \ell n}{\lambda_o} \tag{26}$$

where λ_o is the free space optical wavelength. The variation of phase delay with respect to the variation of n is

$$d\phi = \frac{2\pi \ell}{\lambda_o} dn. \tag{27}$$

If n is varied with respect to time in a controlled manner then the phase delay is also varied directly and a means of phase-modulating an optical beam exists.

From standard FM analysis it is known that the phase modulated wave consists of a carrier and sidebands which are separated by ω_m where ω_m is the angular frequency of the modulating mechanism, in this case the angular frequency of the variation in the index of refraction of the slab of material. The amplitude of the carrier and the sidebands vary as Bessel functions where J_o corresponds to the carrier, J_1 to the first sideband, etc.

When an acoustical wave is launched in a medium and an incident optical wavefront passes through the medium as in Figure 11, modulation will occur. The acoustical wave launched in the modulator with angular frequency ω_m and at the acoustical velocity of the medium V_a, propagates through the modulator with variations of compression and rarefactions with an acoustical wavelength λ_a

$$\lambda_a = \frac{2\pi V_a}{\omega_m} \quad . \tag{28}$$

The rarefactions and compressions cause the corresponding variations in the index of refraction. These "slabs" of different indices of refraction modulate the incident optical wavefront yielding the carrier and sidebands of which the carrier and first upper order are illustrated in Figure 11 [10].

The first upper diffracted wave is indicated in Figure 11. Higher order upper sidebands are tilted up at a greater angle and the lower order sidebands are tilted down. Figure 12 shows the Debye-Sears effect and the variation in the index of refraction in the modulator.

3. Bragg Diffraction

If the wavefront variation in the index of refraction is characterized as a partially reflecting mirror and the optical beam is incident upon the acoustical wavefront at an angle θ_i as is shown in Figure 13 [9] then the diffracted wave will be directed away with the angle of refraction θ_r. A necessary condition for diffraction in a given direction

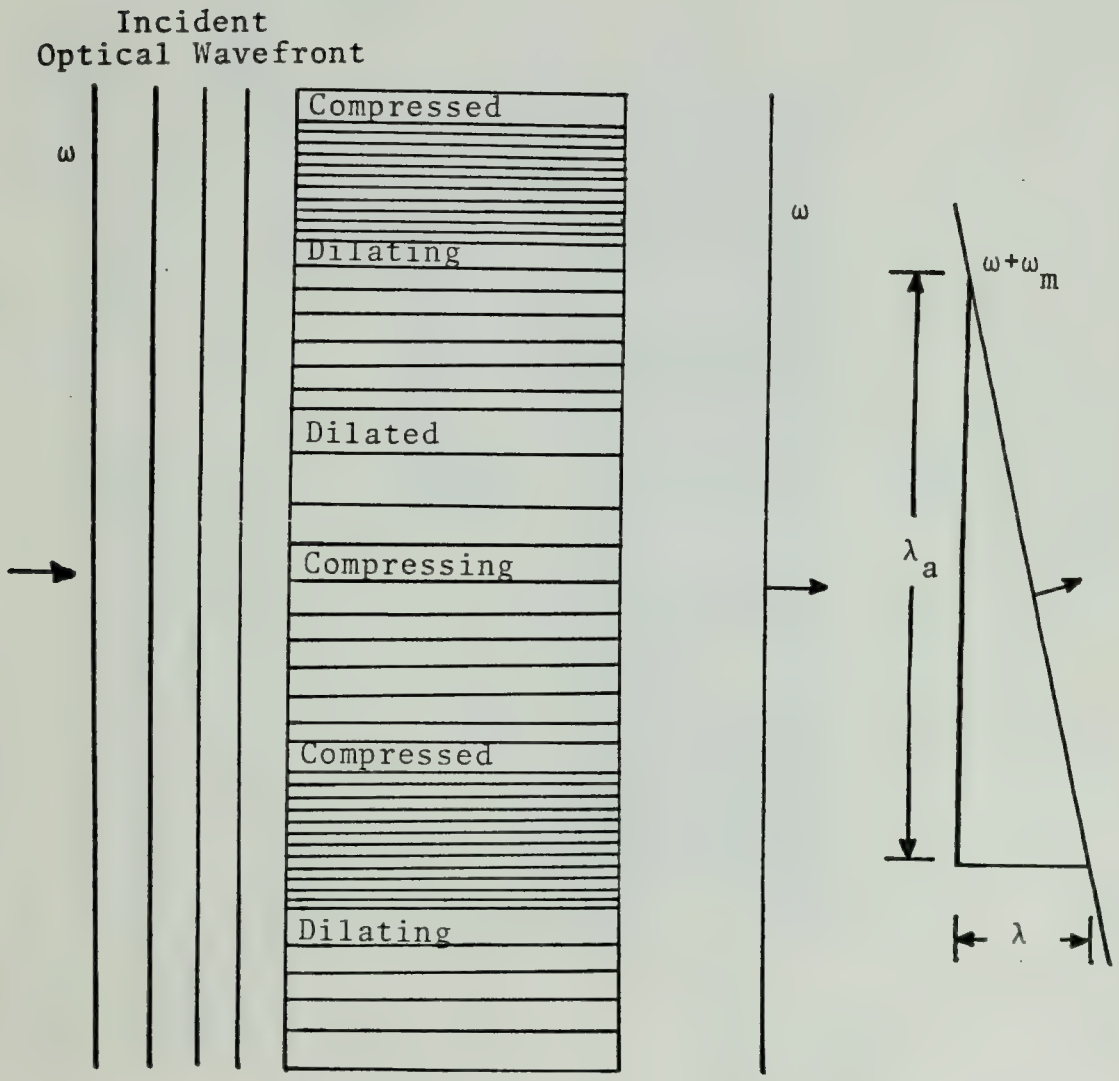

Figure 11. Debye-Sears Effect.

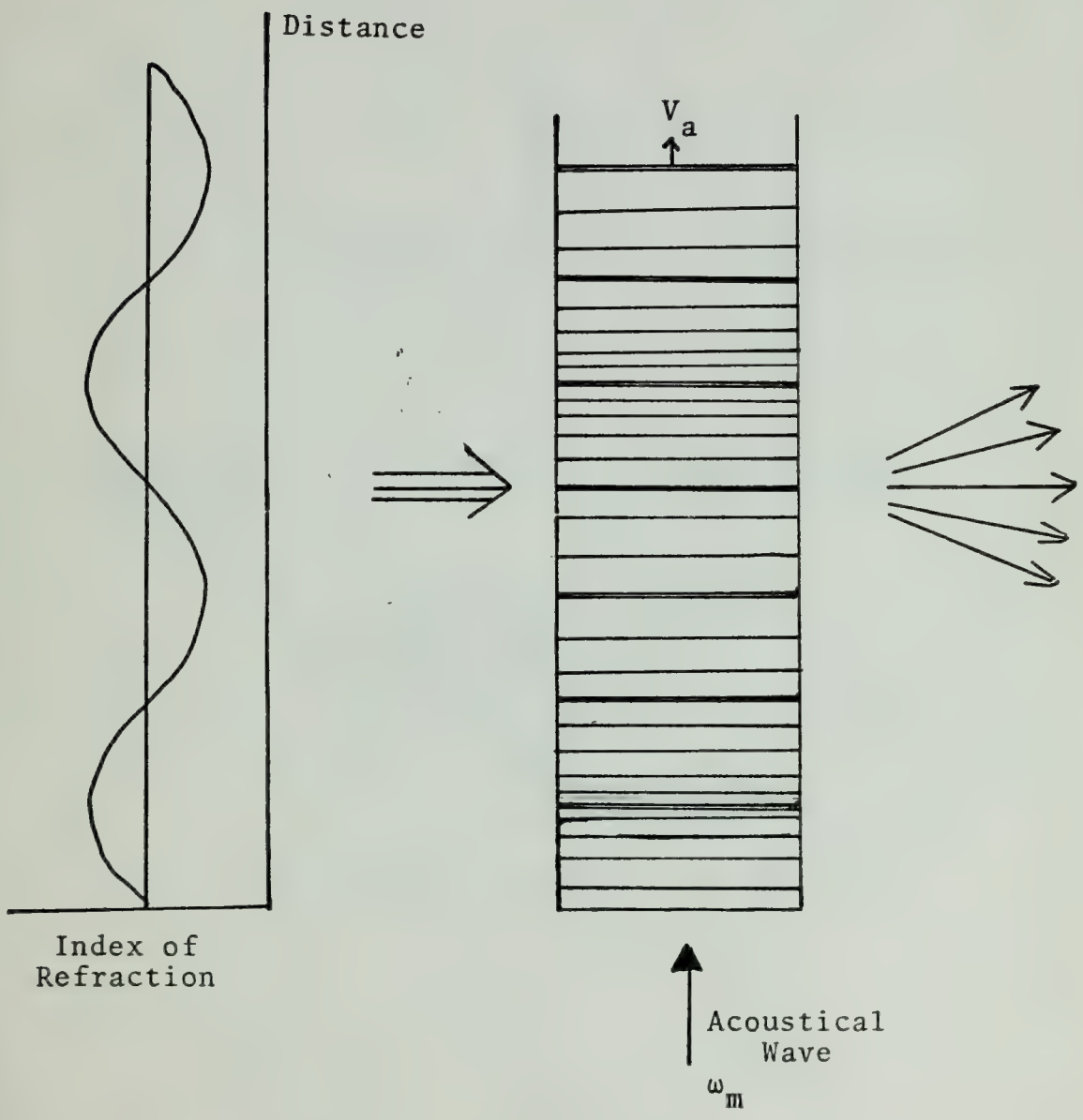

Figure 12. Debye-Sears Effect.

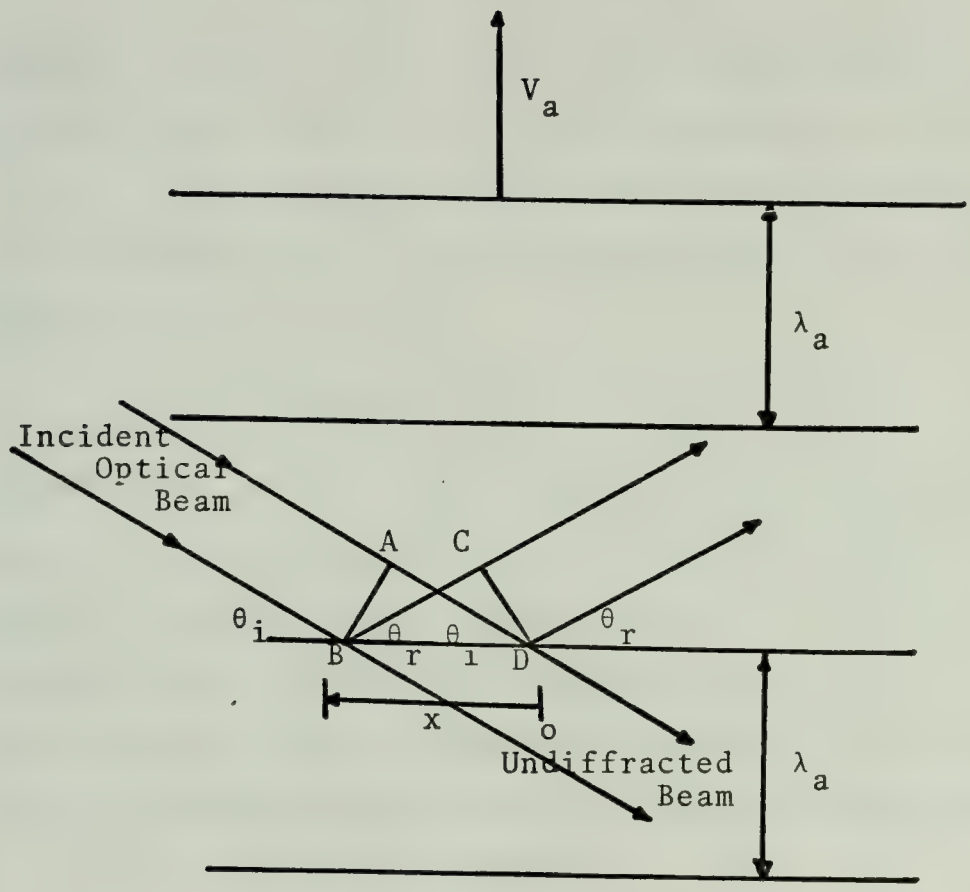

Figure 13. Bragg Diffraction.

is for all points on the reflecting surface to contribute in phase. To satisfy this requirement for the two points of diffraction B and D the difference between the paths AD and BC must be an integral multiple of the optical wavelength λ_o. This condition is satisfied when

$$x(\cos\theta_i - \cos\theta_r) = m\lambda_o \tag{29}$$

where m = o, ±1, ±2,... This can be satisfied for all points x only when m = o. This requirement indicates that $\theta_i = \theta_r$. Additionally for different wavefronts of the modulator (separated by λ_a) to interfere constructively it is required that

$$2\lambda_a \sin\theta = \lambda_o \tag{30}$$

where $\theta_i = \theta_r = \theta$. This is known as Bragg diffraction since it is the same requirement for X-ray diffraction in a lattice Since λ_a is much larger than the optical wavelength, λ_o, $\sin\theta$ is small and is usually approximated by θ. It is also seen from Figure 13 that the angular separation between the diffracted and undiffracted beam is twice the Bragg angle θ.

a. Modulation Frequency

Determination of the frequency shift in the diffracted beam can be determined from two approaches. The first is a somewhat simplistic consideration of geometry and doppler shift and the second a consideration of energy and momentum requirements through the utilization of wave vectors.

(1) Dopper Modulation Determination. The acoustical wavefronts which cause diffraction as shown in

Figure 13, are propagating through the acousto-optic modulator with velocity V_a. This will yield a doppler shift in the diffracted beam according to the relationship

$$F_{doppler} = \frac{2V_a \sin\theta f}{c} \tag{31}$$

where f is the optical frequency. From the Bragg equation (30) the relationship between $\sin\theta$ and the two wavelengths are shown. The doppler shift is given by

$$F_{doppler} = \frac{2V_a \lambda_o f}{2\lambda_a} = \frac{V_a}{\lambda_a} = F_m \tag{32}$$

where F_m is the frequency of the acoustical wave. If the two wavefronts are closing as is shown in Figure 13 the doppler shift is positive and the frequency of the diffracted wave is $F+F_m$. If the relative velocity between the two wave fronts is negative the frequency of the diffracted wave is $F-F_m$.

(2) Particulate Analysis of Modulation. Light has a dual wave-particle nature and analysis can be done by consideration of its particulate nature. Photons have an energy $h\omega$ and momentum $h\vec{k}$. Similarly the acoustic phonons have an energy $h\omega_a$ and momentum $h\vec{k}_a$. In any interaction between the photons and phonons both energy and momentum must be preserved since both the incident photon and phonon cease to exist and a new diffracted photon is created. Figure 14 shows the wave vector relationship between the incident photons $\vec{k}_i$, the diffracted photon $\vec{k}_r$ and the acoustical phonons $\vec{k}_a$. Conservation of momentum requires that

$h(\vec{k}_a+\vec{k}_i)$ of the colliding phonon and photon equal $h\vec{k}_r$ of the scattered photon,

$$\vec{k}_r = \vec{k}_s + \vec{k}_i. \tag{33}$$

Conservation of energy requires

$$\omega_r = \omega_i + \omega_a = \omega + \omega_m \tag{34}$$

or for a negative relative velocity

$$\omega_r = \omega_i - \omega_a = \omega - \omega_m \tag{35}$$

which shows that the diffracted wave is modulated by the acoustic frequency.

Since the acoustic frequencies are less than 10^{10} and the optical frequencies are greater than 10^{13}

$$\omega_r = \omega \pm \omega_m \simeq \omega, \quad \text{so } |\vec{k}_r| \simeq |\vec{k}_i| \tag{36}$$

and the magnitude of the two optical wave vectors is approximately the same. From Figure 14 it is seen that

$$|k_a| = 2|k_i|\sin\theta \tag{37}$$

and since

$$|k_a| = 2\pi/\lambda_a \tag{38}$$

it follows that

$$2\lambda_a\sin\theta = \lambda_o \tag{39}$$

which is the Bragg diffraction requirement.

Figure 14 is for perfectly monochromatic plane waves. In actuality there is both wave divergence and some frequency variation. Thus rather than being only one exact angle of diffraction allowed there is a small range. This

effect is illustrated in Figure 15 where only acoustical divergence is considered [11].

4. Modulation Bandwidth

The modulator bandwidth is inversely proportional to the transit time of the acoustic wave across the optical beam. A means of increasing the bandwidth is to focus the optical beam and have its waist centered in the modulating medium. The waist diameter can be determined from the relationship [12]

$$w_o = \left(\frac{2\ell n2}{\pi} \right) \frac{F\lambda}{W_o} \tag{40}$$

where w_o is the focused optical waist diameter, W_o is the unfocused beam waist and F is the focal length of the focusing lens. The expression for modulator bandwidth is given by [13]

$$\Delta f \simeq .54\ V_a/W_o \tag{41}$$

where V_a is the acoustical velocity.

5. Modulation Power Transfer

The amount of power transferred from the incident beam to the modulated beam is a direct function of interaction length ℓ of the beam through the modulating medium and the amount of change of the index of refraction in the medium. The latter is a direct function of the acoustical power up to a saturation level in the medium. This power transfer is also inversely related to the optical wavelength. In the previous section it was noted that the modulating bandwidth is inversely proportional to the optical waist

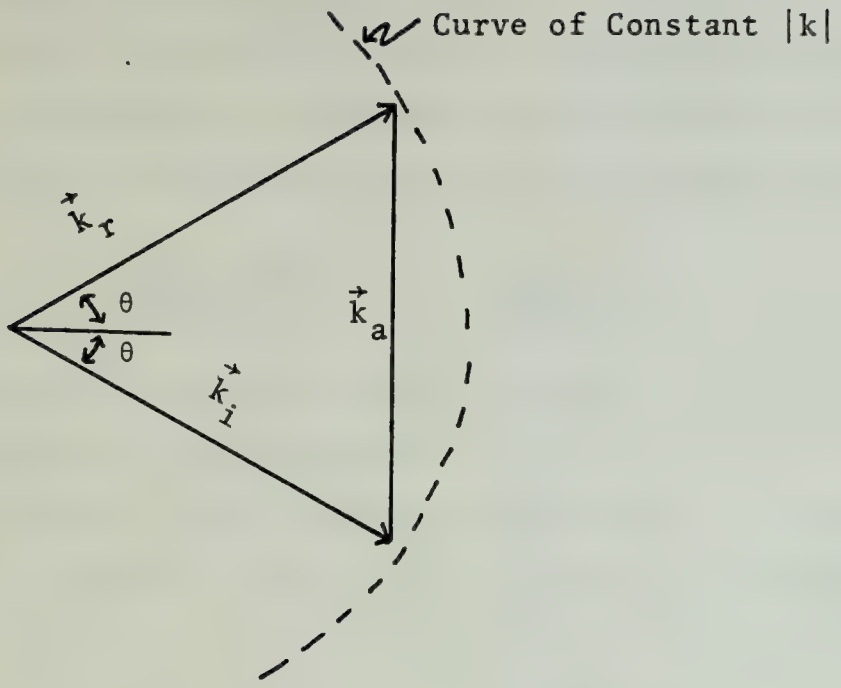

Figure 14. Momentum Scattering for Plane Monochromatic Optical and Acoustical Waves.

Figure 15. Momentum Scattering for Acoustical Waves of Finite Width and Diffraction.

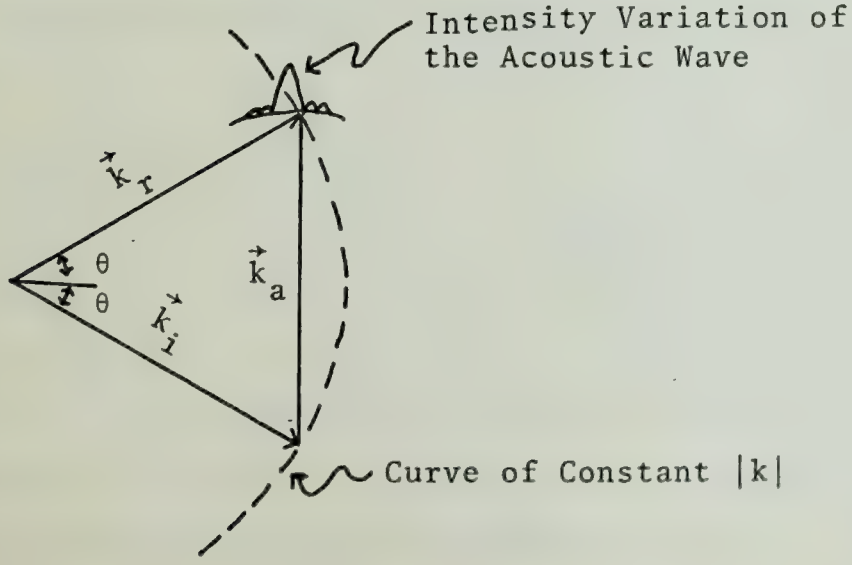

diameter, there is a tradeoff between the waist diameter and the length that the optical wavefront is planar so this must be considered with respect to the diffraction efficiency. The expression for diffraction efficiency is given in (3). With some manipulation this reduces to

$$\frac{I_{diffracted}}{I_{incident}} = \sin^2 \left(\frac{\pi \ell \Delta n}{\lambda_o} \right) . \qquad (42)$$

Another approach to this is given in [14].

6. Modulator Considerations

A diagram of an acousto-optic modulator is shown in Figure 16. There is a transducer to couple the electrical modulating signal into the crystal. To date the transducer is often the limiting component with respect to the bandwidth. At the opposite end of the modulating crystal there is an absorbing medium to prevent reflection of the acoustical waves back into the optical beam.

C. DETECTION

Detection of optical signals encompasses many aspects however, only those pertinent to the CO_2 laser radar will be covered.

1. Photo-Voltaic Detector

Photo-Voltaic detectors are semiconductor diodes in which incident photons create electron-hole pairs in or within one diffusion length of the depletion region of the diode. These generated carriers are accelerated in opposite directions by the intrinsic field present within the depletion region and depending upon biasing arrangement, give a signal

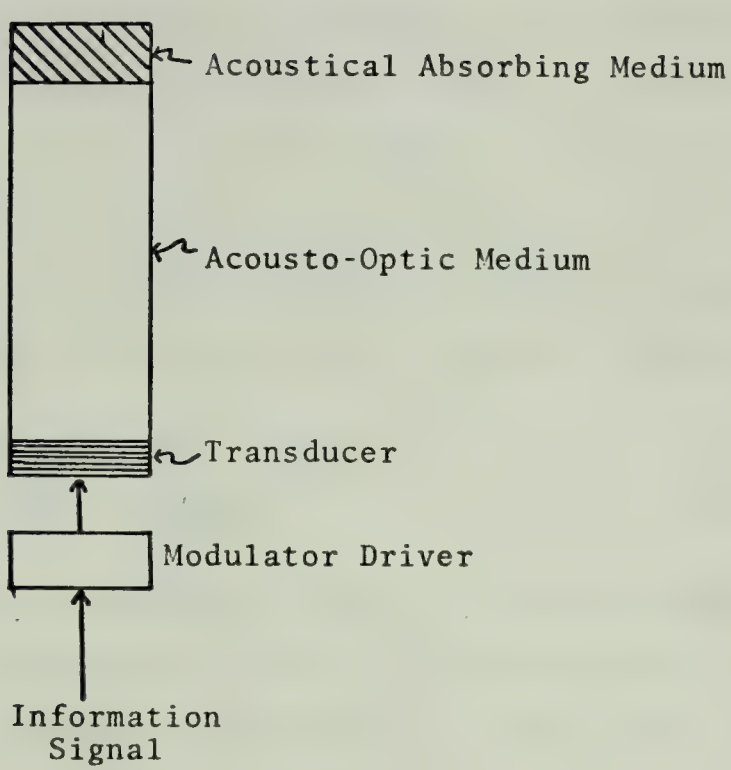

Figure 16. Acousto-Optic Modulator.

either in current flow variation or output voltage variation. In properly constructed and biased diodes the generated excess carriers move at scattering limited velocity and there is virtually no recombination within the depletion region.

a. Spectral Response and Quantum Efficiency

The absorption of photons in the semiconductor material is a strong function of the wavelength of the incident photon. To a much lesser degree there is variation with temperature since both the semiconductor energy gap and surface recombination velocity are effected by temperature. The maximum wavelength that will generate an excess carrier in the semiconductor material is given by the relationship [15]

$$\lambda_c = \frac{hc}{E_g} = \frac{1.24(\mu m)}{E_g(eV)} \tag{43}$$

where λ_c is the cut-off wavelength and E_g is the forbidden energy gap. Wavelengths longer than λ_c will effectively pass through the active region of the photodiode without absorption.

Shorter wavelength photons will be more readily absorbed until for much shorter wavelengths the photons are essentially all absorbed very near the semiconductor surface and the generated excess carriers are lost to the detection process due to high surface recombination that occurs near the boundaries of the crystal lattice. The overall effect of the wavelength dependency of photon absorption yields a curve as is shown in Figure 17. This shows the effective quantum efficiency of intrinsic silicon and germanium photodetectors.

The quantum efficiency is a measure of the conversion efficiency of the photodetector in converting photons to excess carriers. Quantum efficiency, η, is defined as the ratio of the number of photons that generate excess carriers to the number of photons incident upon the detector. The current generated in a photodiode is given by

$$i = \eta q \Phi A \tag{44}$$

where η is the quantum efficiency, q is the electronic charge, Φ is the incident photon flux density and A is the active area of the detector.

The equivalent circuit of a photodetector is given in Figure 18 [15]. The available power into a matched load from this circuit is [15]

$$P_{avail} = \frac{1}{8}|I_{PD}(\omega)|^2 \frac{1}{\omega^2 c^2 R} \tag{45}$$

$$= \frac{1}{8}(\eta q \Phi A)^2 \frac{1}{\omega^2 c^2 R} . \tag{46}$$

Due to thermally generated carriers known as dark current all semiconductor detectors which operate at 10.6 μm must be cooled to 77°K. Due to advances in material processing this requirement may be relaxed somewhat.

b. Detector Noise

There are three primary categories of noise in photodetectors, all of which predominate in a general frequency range.

(1) 1/f Noise. There are several types of noise for which the power spectrum varies as the inverse of frequency. This noise is sometimes known as modulation

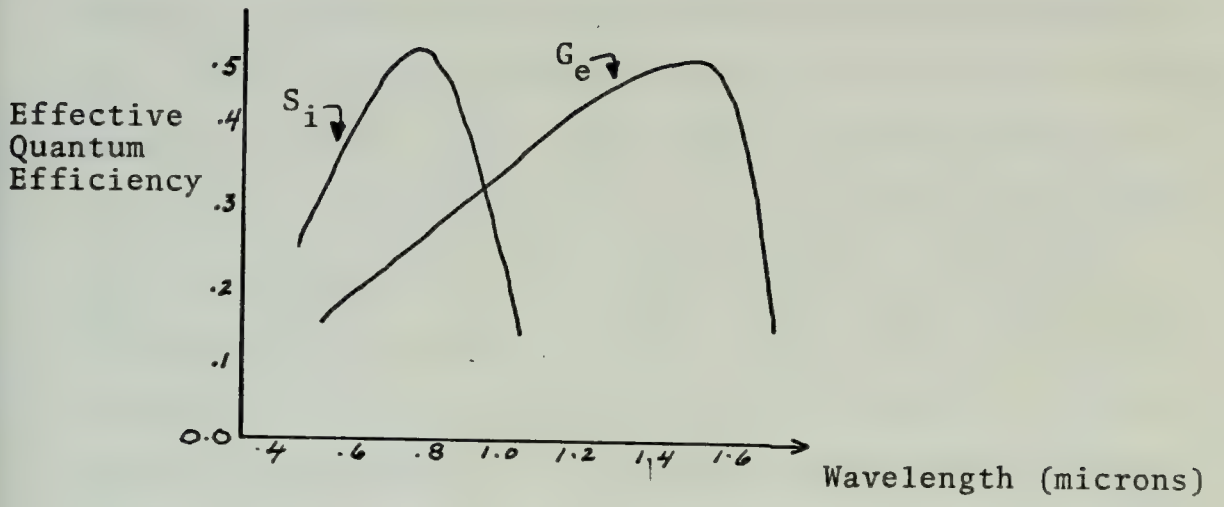

Figure 17. Effective Quantum Efficiency vs. Wavelength for G_e and S_i Photodetectors.

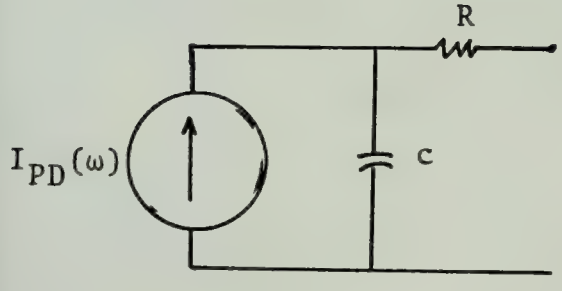

Figure 18. Equivalent Circuit of a Photodiode.

noise in semiconductors or flicker noise in vacuum tubes. 1/f noise becomes negligible with respect to other noise sources above a few kHz.

(2) Generation-Recombination (g-r) Noise. In semiconductors the major source of noise at intermediate frequencies (above the range where 1/f noise predominates) is g-r noise which is due to fluctuations in rate of charge carrier generation and recombination. This variation is due in part to the randomness of the arrival of the photons of the incident flux. This latter effect is sometimes categorized separately as photon noise. Generation-recombination noise is relatively flat with respect to frequency up to the value where it is approximately equal to the inverse of the free carrier lifetime; at this point it falls off at about 6 db per octave.

(3) Johnson Noise. Johnson noise is thermally generated and present in all devices in accordance with their temperature and bandwidth. The noise is independent of frequency up to extremely high frequencies. The expression for thermal noise power is given by [16]

$$\text{Noise}_J = \frac{4kTB}{R} \tag{47}$$

where k is Boltzmans constant, T is the temperature in degrees Kelvin, B is the device bandwidth and R is the device resistance. A profile of noise contribution as a function of frequency from [17] is given in Figure 19.

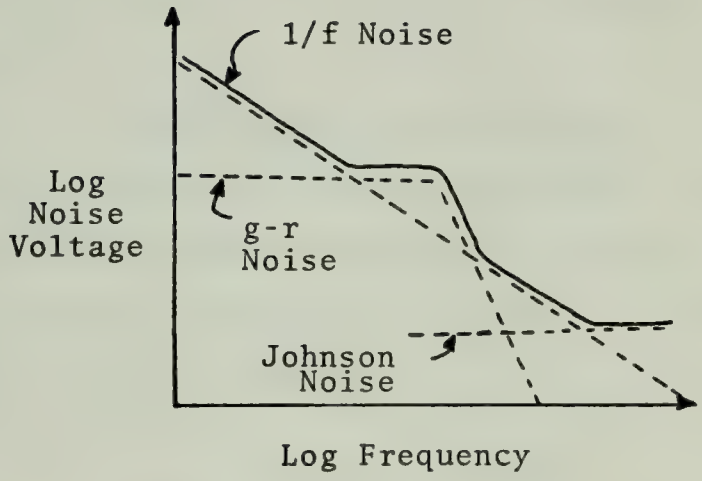

Figure 19. Generalized Detector Noise Spectrum.

c. Detector Characterization

There are several figures of merit which are useful in describing photodiode performance. Those which are significant with respect to the laser radar are R, NEP and D^*.

(1) Responsivity. Responsivity, (R), is a measure of a detector's output for a given input. The units of responsivity are v/w and it is given by

$$R = \frac{V_s}{HA_d} \tag{48}$$

where V_s is the r.m.s. signal voltage, H is the r.m.s. value of the irradiance on the detector and A_d is the detector area in cm^2.

(2) Noise Equivalent Power. A more meaningful detector parameter is noise equivalent power, (NEP). NEP is the radiant flux necessary to provide an output signal such that the signal to noise ratio is equal to one. NEP can be calculated from

$$NEP = \frac{HA_d}{(V_s/V_n)^2} = \frac{HA_dV_n^2}{V_s^2} \tag{49}$$

where V_n is the noise voltage, V_s is the signal voltage and H and A_d are as in (48). A good photodiode will have a NEP of 10^{-19} - 10^{-20} w. In shot noise limited heterodyne operation the NEP of a photodiode is [18]

$$NEP = \frac{hfB}{\eta} . \tag{50}$$

(3) $\underline{D^*}$. Since both signal and noise are a function of detector area and noise is a function of bandwidth a measure accounting for these factors is D^* (dee-star).

$$D^* = \frac{(A_d B)^{\frac{1}{2}}}{NEP} . \qquad (51)$$

B is the detector bandwidth and A_d is the detector area. The units of D^* are $cmHz^{\frac{1}{2}}w^{-1}$ and the measurements are usually taken at peak responsivity. The theoretical limit of D^* for a photodiode at 10.6 μm viewing a hemispherical surrounding at 300°K is approximately 5×10^{10}. A good detector at 10.6 μm will have a D^* of about 2 or 3×10^{10} $cmHz^{\frac{1}{2}}w^{-1}$.

2. Coherent Detection

Optical signal processing is available in photodiodes by heterodyne or coherent detection. Alignment of the phase fronts of the signal and local oscillator beams is extremely critical and anything which causes phase front distortions severely degrades detection.

In the detector the shot noise due to the local oscillator power can be made to override all other noise sources. Operation in this condition is known as shot noise limited operation and this condition allows detection of signals down to a theoretical minimum known as quantum limited operation. Neglecting the noise contribution due to dark current (at 77°K the amount of dark current is very small) the power signal to noise ratio for heterodyne detection in a photodiode is [19,20]

$$\frac{S}{N} = \frac{2(\eta q/hf)^2 P_L P_S}{\left[\frac{2q^2\eta}{hf}(P_L+P_S+P_B) + \frac{4kT_D}{R_D} + \frac{4kT_A}{R_L}\right]B} \qquad (52)$$

where T_D and T_A are the detector and amplifier temperatures and P_L is the local oscillator power, P_S is the signal power, P_B is the power due to background radiation and B is the system bandwidth. The numerator is the power of the difference frequency component of the detector output signal and the denominator consists of the shot noise power and thermal noise power.

In shot noise limited operation the power of the local oscillator is increased until its power is greater than the signal and background power and the shot noise due to the local oscillator dominates all other noise contributions. At this level the signal to noise ratio becomes

$$\frac{S}{N} = \frac{\eta P_S}{hfB} . \qquad (53)$$

This is twice the SNR of a shot noise limited photoconductor [21].

For homodyne operation the signal to noise ratio is doubled and is [14]

$$\frac{S}{N} = \frac{2\eta P_S}{hfB} . \qquad (54)$$

The value of heterodyne SNR given in (53) is for optimal phase front alignment. If misalignment is due to angle of incidence in only one coordinate the amount of misalignment which will degrade the heterodyning efficiency by 10% or less is [14]

$$\psi \leq \frac{\lambda}{4d} \tag{55}$$

where ψ is the amount of angular misalignment, λ is the optical wavelength and d is the detector size. For a 10 mil detector at 10.6 μm

$$\psi \leq 10.4 \text{ mrad.}$$

D. ATMOSPHERIC PROPAGATION

The propagation medium for an optical radar is the atmosphere which affects the transmitted and return beam in several ways.

1. Transmissivity

Energy attenuation in the atmosphere is a strong function of wavelength. There are several atmospheric windows which are located in the following approximate ranges: (Figure 20)

.2 - 1.3
1.5 - 1.8
1.9 - 2.6
3 - 4.2
4.5 - 5
8 -13.5.

The attenuation in the atmosphere is a consequence of both absorption and scattering. The transmittance of a path can be expressed as [17]

$$t = e^{-\sigma x} \tag{56}$$

where σ is the extinction coefficient and x is the path length. The extinction coefficient is the sum of the absorption coefficient α which accounts for molecular absorption and the scattering coefficient γ which accounts for scattering

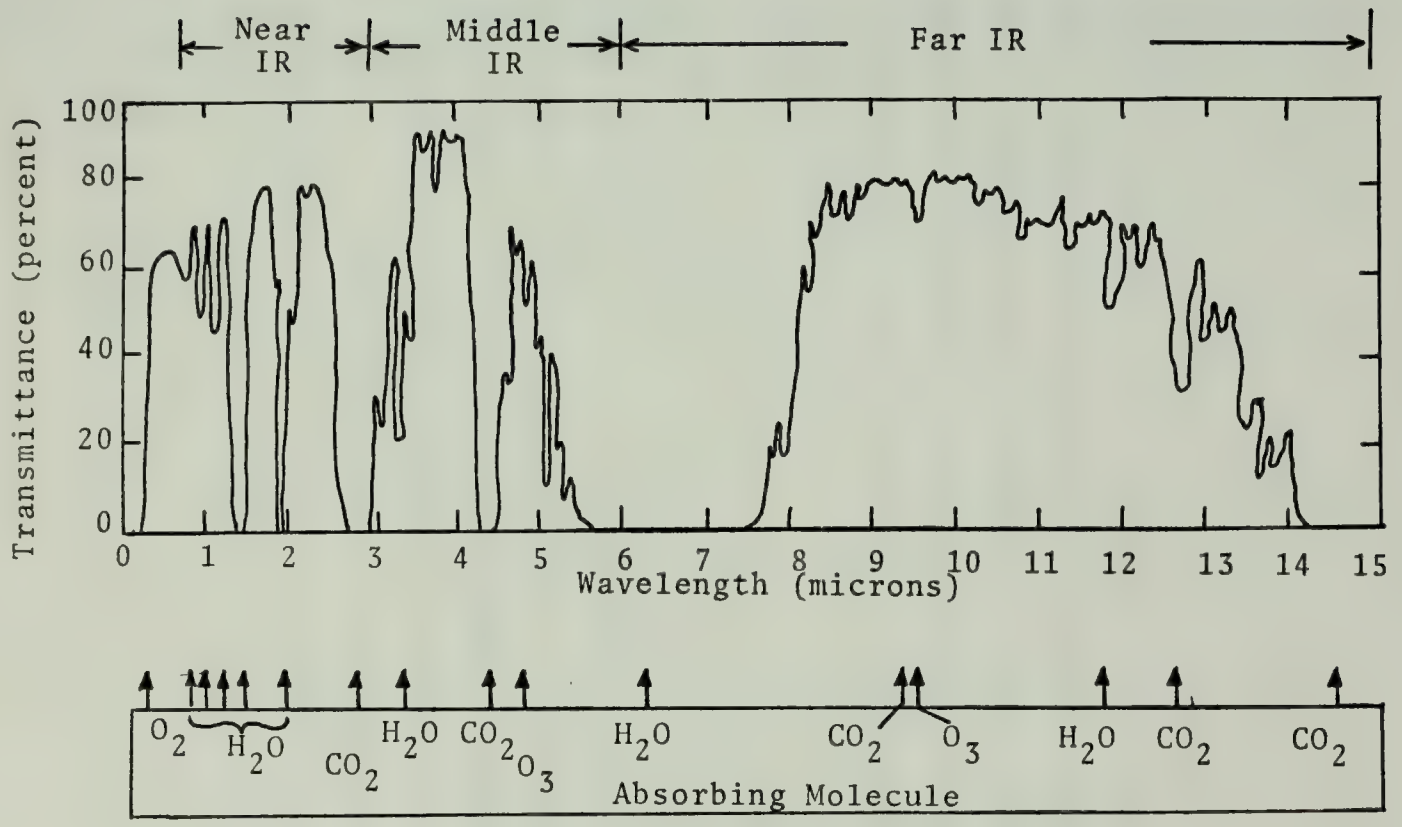

Figure 20. Atmospheric Transmittance as a Function of Wavelength.

by molecules, haze and fog. Both α and γ vary as a function of wavelength, climate conditions, temperature, humidity and altitude.

a. Absorption

In the region of interest (10.6 μm) there are two absorbing molecules which are of significant importance. These molecular absorbers are CO_2 and H_2O. Water content may vary from as much as 2% of a very humid atmosphere at sea level to a very minor amount in extremely arid regions. The water vapor content of the atmosphere decreases rapidly with altitude until at 40,000 ft it is considered negligible. Water vapor content is also inversely proportional to temperature, thus cold climates or weather minimize the absorption due to H_2O.

Carbon dioxide constitutes approximately .032% of the atmosphere by volume. This percentage is relatively constant up to an altitude of about 30 miles, then decreases by a factor of ten for every 10 miles increase in altitude. CO_2 content varies little with temperature or weather and thus is a much less variable component than water vapor.

There are several other absorbers such as ammonia, carbon monoxide, sulfur dioxide, methane or nitrous oxides which are normally present in negligible amounts. In industrial or polluted regions these gases may be present in sufficient quantities to produce significant attenuation.

b. Scattering

The relationship between the scattering coefficient and wavelength which is often used in predicting transmissivity is [17]

$$\gamma \simeq \lambda^{-\psi} \tag{57}$$

where ψ is a function of the ratio of the particle size to the wavelength. If the particles are small with respect to the wavelength ψ is equal to 4 and the scattering process is known as Rayleigh scattering and is strongly dependent upon wavelength. It is this wavelength dependent scattering which causes the sky to appear blue. For larger particles the value of ψ approaches zero, this process is called Mie scattering and is independent of wavelength. For most fogs ψ is zero for the visible spectrum and thus the fog appears white.

In general the atmospheric categorization of haze consists of particles whose radii range up to .5 μm and that of fog consists of particles which range from .5 - 80 μm with a distribution peak which usually ranges from 5 - 15 μm. These numbers indicate that at 10.6 μm haze will have minimal effect but fog will greatly reduce transmissivity. Actual experience obtained by the Naval Electronics Laboratory Center at San Diego seems to indicate that fog may not scatter as much as was expected.

Rain reduces the transmissivity in direct proportion to its intensity. Raindrops range in size up to approximately 3 mm and thus ψ has a value of zero and Mie

scattering with wavelength independence is the scattering phonomonon. All experience to date indicates that rainfall is the predominate attenuating factor at 10.6 μm.

c. Scintillation

Scintillation is the phenomonon which causes uncorrelated variation of intensity and apparent directional changes in a radiant source. This phenomonon is caused by relatively rapid discontinuous variations in the index of refraction in the propagation path. Scintillation is the primary effect which renders amplitude modulation of an optical beam for atmospheric propagation a poor second choice when compared to frequency modulation.

d. Ray Bending

Variations in the index of refraction of a more continuous nature can cause beam bending. This can cause errors in angular location of targets and other abberations due to ducting as is experienced in more conventional radars.

e. Turbulence

Atmospheric turbulence causes pheonomona such as scintillation and phase front distortion. Turbulence causes variations of intensity and phase across the beam surface. Direct detection [14] allows integration of the intensity variation as the receive aperture increases, but for coherent detection there can be a decrease in signal to noise ratio as aperture size is increased since the variations in phase front degrade the signal rather than integrate out.

III. MAJOR SYSTEM COMPONENTS

A. LASER

The laser utilized in the radar system is a 3 w, vertically polarized CO_2 laser (10.6 μm wavelength) built by Honeywell Corporation. The laser is a closed system laser and is water cooled. It has an internal piezzo-electric transducer (PZT) which allows some modulation and control for line shifting. The PZT was not utilized in the system.

The laser power output as a function of driver setting is given in Table I. The divergence of the laser was computed as 1.71 mrad. This value is somewhat lower than the value estimated by NELC but NELC did not measure the divergence.

A cooling water hose connection inside the laser head came unconnected during operation of the laser. The water caused a short from the high voltage leads (±10 KV) to ground which resulted in the destruction of an inductor in the laser power supply filter. This required operation of the laser with an unfiltered power supply and as a result the output power dropped from 3.05 w to 2.3 w and contained a 120 Hz ripple. The result of this was a drop in peak transmitted power from 1.2 w to .65 w and a drop in unfocused local oscillator power from .93 w to .51 w.

The laser was microphonic (amplified low frequency mechanical vibrations) but this was filtered out in the signal processing and presented no problem.

Driver Supply Setting	Power Output (Watts)
72	.25
76	.64
80	1.1
82	1.25
84	1.5
86	1.7
88	1.95
90	2.15
92	2.3
94	2.45
96	2.54
98	2.68
100	2.76
102	2.89
104	2.95
110 (Max)	3.05

Table I. Laser Output Power as a Function of Driver Setting. (Data taken 18 July 1974)

B. ACOUSTO-OPTIC MODULATOR

The acousto-optic modulator utilized in the system is made by Isomet. Its specifications are listed in Table II [22]. The crystal is germanium and both the modulator and driver are RFI hardened. A sketch of the modulator is shown in Figure 21. Table III shows the modulation frequency as a function of input voltage. While the laser power supply was filtered the modulator was frequency modulated from 35 - 45 MHz and the modulated output power was 1.2 w while the unmodulated beam power was .93 w for a modulating efficiency of 56%. During unfiltered operation the efficiency was unchanged. This performance was completely satisfactory considering that the Bragg angle varies with frequency and the modulator angle was held constant at approximately 2.2° (the Bragg angle for 40 MHz operation).

The modulator crystal is germanium which has an acoustical velocity of 5.4×10^5 cm/sec [23]. This yields an acoustical wavelength at 40 MHz of 135 μm.

There are two 5 inch focal length focusing lenses with the modulator. The first is to focus the incoming beam to a minimum waist size to increase the modulator bandwidth and the second lens is to recollimate the output beams.

There is a time delay between the driver output and the interaction of the acoustical and optical beams. This propagation delay in the crystal is due to the time delay required to propagate from the transducer to the optical beam and gives an additional frequency offset to the range frequency. In earlier system alignments this time delay

Modulator	
Operating wavelength	10.6 μm
Rise time	70 nsec
Deflection efficiency	> 60% with DC input
Contrast ratio	1000:1
Static transmission efficiency	88%
Coatings	AR at 10.6 μm
Optical aperture	1 mm
Acoustic center frequency	40 MHz
Nominal impedance	50 Ω
Cooling	water cooled
Driver	
Bandwidth	35 - 45 MHz
Input impedance	50 ohms
Linearity	> 5% deviation
Input voltage	- 6.27v (35 MHz) to - 9.27v (45 MHz)
Output amplitude variation	± 1 db

Table II. Acousto-Optic Modulator Characteristics.

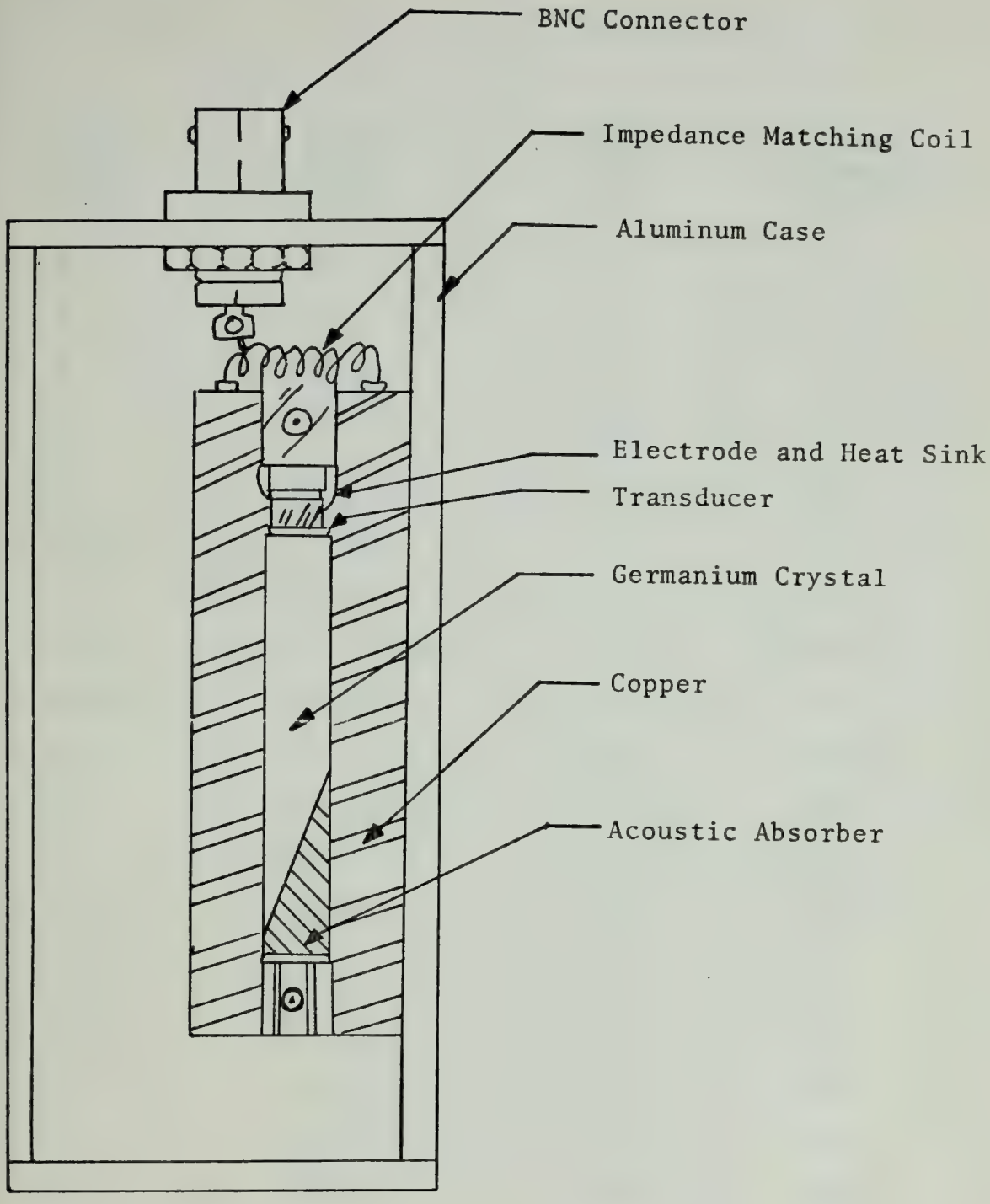

Figure 21. Acousto-Optic Modulator.

Input Voltage (V)	Output Frequency (MHz)	Input Voltage (V)	Output Frequency (MHz)
6.0	35.2	8.1	42.1
6.1	35.6	8.2	42.4
6.2	35.9	8.3	42.8
6.3	36.2	8.4	43.1
6.4	36.6	8.5	43.4
6.5	37.0	8.6	43.7
6.6	37.3	8.7	44.0
6.7	37.6	8.8	44.3
6.8	37.9	8.9	44.6
6.9	38.3	9.0	44.9
7.0	38.6	9.1	45.2
7.1	38.9	9.2	45.5
7.2	39.2	9.3	45.8
7.3	39.6	9.4	46.0
7.4	39.9	9.5	46.3
7.5	40.2	9.6	46.6
7.6	40.5	9.7	46.9
7.7	40.8	9.8	47.1
7.8	41.2	9.9	47.4
7.9	41.5	10.0	47.7
8.0	41.8		

Table III. Modulator Frequency as a Function of Input Voltage.

was approximately 1.6 μs which translates to a frequency offset of 56 kHz. After realignment and repositioning of the height of the modulator the delay was approximately 1 μs which corresponds to 35 kHz. A 1 μs delay corresponds to 5.4 mm travel through the crystal.

C. DETECTOR

The detector used in the system was a PbSnTe heterojunction p-i-n photodiode made by Rockwell International Science Center [19]. The detector area was 4×10^{-4} cm^2 and operation at liquid nitrogen temperatures (77°K) is required.

The zero bias quantum efficiency was listed as .14 with a peak quantum efficiency of .32 with .2 v bias (Table IV). The measured zero bias quantum efficiency was .034. No reason is known for this change except apparent detector degradation. Some of the personnel at NELC expressed the opinion that the detector had degraded. Determination of quantum efficiency in heterodyne operation indicates a biased quantum efficiency of approximately .12.

Shot noise limited operation was not achieved with the detector. An estimated local oscillator power incident upon the detector was .1 mw. The detector dynamic impedance varies with biasing but with zero bias the resistance is approximately 50 Ω. Using a quantum efficiency of .14 either signal or local oscillator power greater than .9 mw would be required. For a quantum efficiency of .034 greater than 3.7 mw would be required. This exceeds the incident power capability of the detector (3 mw).

Bias Voltage (Volts)	3 db Bandwidth (MHz)	Quantum Efficiency (%)
0	200	14
.02		20
.05		27
.1		30
.15	200	
.2		32
.3	200	
1.0		32

Table IV. Detector 3 db Bandwidth and Quantum Efficiency vs. Bias Voltage [19]

The 3 db bandwidth is listed as 200 MHz. The maximum frequency at which the detector was operated was 55 MHz. No roll-off due to frequency response was noted.

The detector was mounted in a stainless steel SAT dewar with a side looking window. The window transmissivity is unknown but a transmissivity of .8 was estimated for calculation purposes.

D. OPTICAL ANTENNA

The special antenna utilized in the radar system is a dual transmit/receive Newtonian lens system [24]. Figure 21 is a diagram of the lens system. The antenna has the following parameters:

Dual antenna - transmits and receives

Transmit/receive folding mirror - double flat parallel surfaces elliptical $1\frac{1}{2}$" x $2\frac{1}{8}$"

Receive aperture mirror - 6" diameter parabolic, 60" focal length

System f/no - 10

Effective f/no (due to blockage)[17]- 10.45

The system yields the following system performance capabilities for diffraction limited optics:

Airy disc diameter [25] $d = 2.44\lambda(f/o) = 259\ \mu m$ (58)

Due to blockage of transmit ellipse [17] $d = 270\ \mu m$

Depth of focus $x = 4\lambda(f/no)^2 = 4.24$ mm (59)

Near limit of field to achieve airy disc

$$x_f = D^2/2\lambda = 1096 \text{ m} \simeq 1199 \text{ yd} \quad (60)$$

Field of view for detector diameter equal to airy disc [17]

$$\beta = d/f = 170\ \mu rad \times .01° \tag{61}$$

Field of view for 8 mil detector [14]

$$\beta = \theta_r = \frac{2.44 \cdot \lambda \cdot d_{detector}}{d_{airy} d_{mirror}} = 127\ \mu rad \tag{62}$$

Angular target resolution

$$\alpha = \frac{.122\lambda}{D} = 85\ \mu rad \simeq .005°. \tag{63}$$

Maximum allowable incident angular wavefront misalignment between signal and local oscillator beam for 10% heterodyning degradation using an 8 mil diameter detector: [26]

$$\psi = \frac{\lambda}{4d} = .013\ rad \simeq .75° \tag{64}$$

Receive aperture = $\pi(6/2)^2 = 28.3\ in^2$

Folding mirror surface = $\pi(3/4)^2 = 1.77\ in^2$
(blockage area somewhat larger)

Percent blockage - $\simeq$ 7%

In the above relationships λ is the optical wavelength of 10.6 μm, f is the focal length (60") and D is the receive mirror diameter.

To transmit directly ahead of the optical antenna the elliptical flat is turned 45° with respect to the antenna axis and the transmit beam comes in at 90° with respect to the antenna axis (Figure 22).

To provide a visible indication of the CO_2 beam location a HeNe laser beam at 632.8 nm is being transmitted aligned with the 10.6 μm beam. As can be seen in photographs (Figures

27, 28 and 29), there is a rifle scope trained on the mirror through which the HeNe beam enters the transmit system. The scope view follows the transmit beams and allows specific location of the output beams. When the system is aligned beam steering by moving the optical table will not require any additional alignment.

Receive alignment can be accomplished by looking into the receive folding surface of the elliptical mirror. Receive view can be determined by moving horizontally and vertically and insuring the target is in the center of the elliptical mirror blockage.

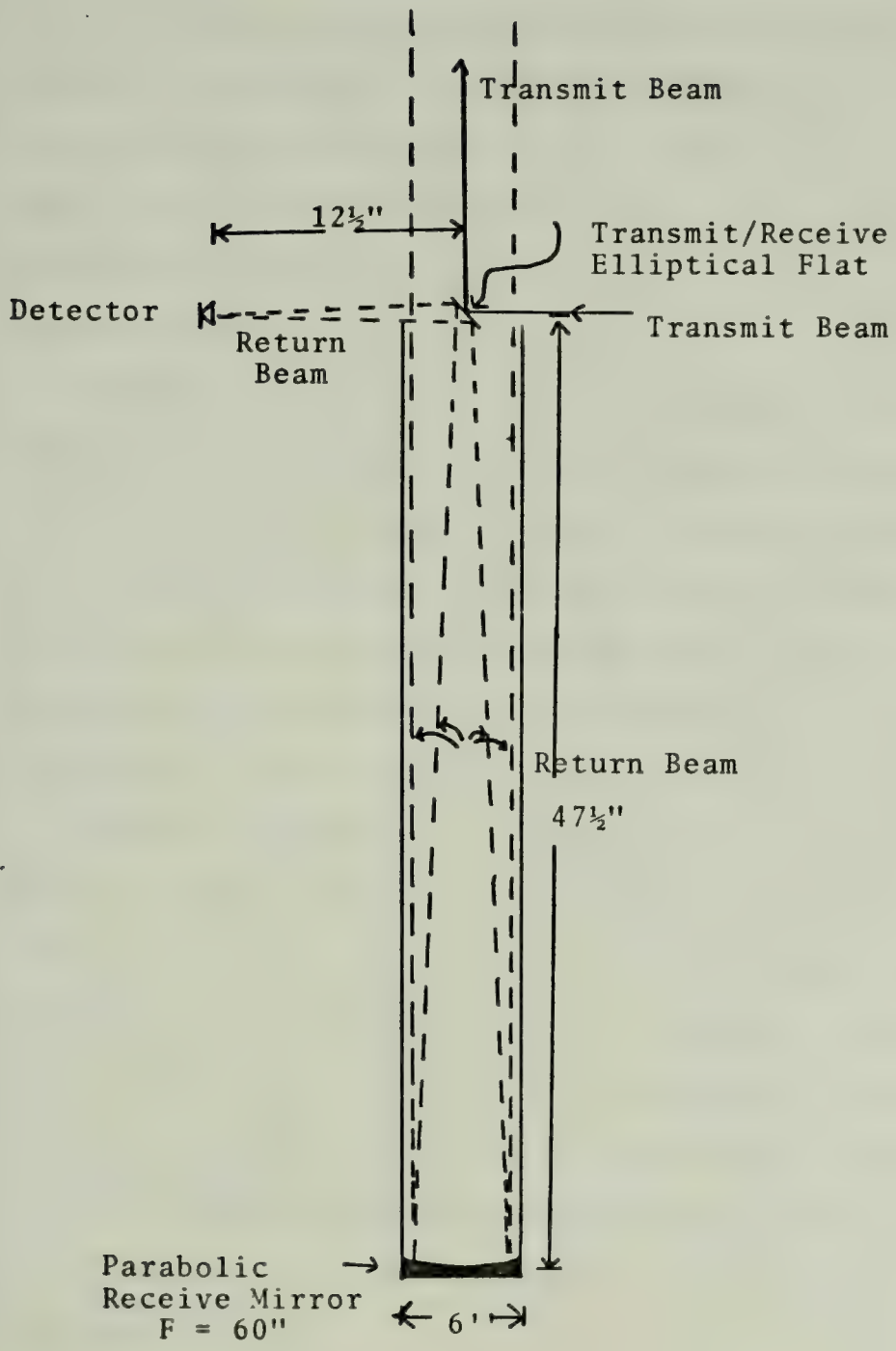

Figure 22. Newtonian Optical Antenna.

IV. SYSTEM ANALYSIS AND ALIGNMENT PROCEDURES

A. PRELIMINARY DEVELOPMENT

The radar system development proceeded through several stages. The initial step was the assembly and alignment of a system which would modulate the laser beam, transmit the beam, receive the return and utilizing heterodyne detection extract the modulated signal. Figure 23 shows the initial system utilized to accomplish this.

Alignment of the system is very crucial and is somewhat complicated by the fact that the CO_2 beam at 10.6 μm is invisible. The presence of the CO_2 beam can be determined by using heat sensitive graph paper or heat sensitive plastic encapsulated liquid crystals. The graph paper is used when the power is relatively high and the liquid crystal paper is utilized for powers down to a few milliwatts.

The beam splitters utilized are germanium with one side anti-reflection coated for 10.6 μm wavelength. The germanium lens and splitters are opaque to visible light. The values listed for the beam splitters first show the reflectance then transmittance. A 90/10 splitter means that 90% of the CO_2 beam is reflected and 10% is transmitted through the splitter. Unless indicated otherwise the lenses, splitters and mirrors are 2 inches in diameter. All mirrors are front surfaced.

Beam splitters provide a means of separating portions of a beam into known components or combining two beams together

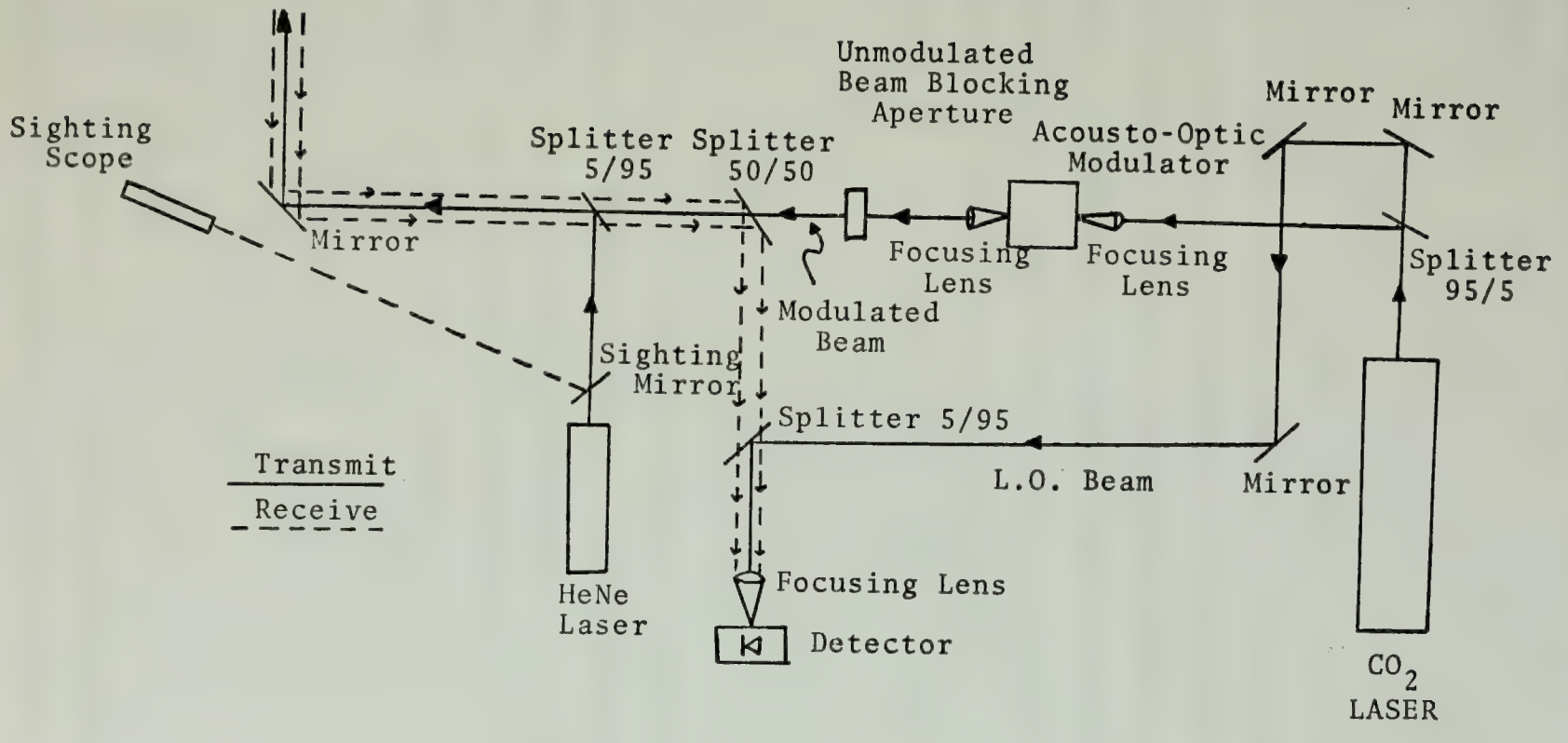

Figure 23. First Optical System.

for collimated joint transmission. One effect of using beam splitters is that to split and combine beams the reflecting surfaces must be at an angle to the beam paths, for a right angle deflection the surfaces must be oriented at a 45° angle with respect to the transmission path. The angular presentation of the surfaces reduces the amount of surface area available for transmission or reflection and at 45° the circle presents an apparent ellipse with a horizontal minor axis of 1.4 inches. The transmittance or reflective area is reduced by the angular presentation to .707 of the original, or in other words, a 1.5 db reduction. This reduction in size presents no problem for the transmit path but for the return path it can reduce the collected energy by 1.5 db.

The holders for the splitters and mirrors have uncoupled horizontal and vertical rotational mobility which allows exact direction of reflected beams. Additionally the A-O modulator and detector holders have 3 degree uncoupled axis mobility with micrometer adjustment for up to one inch travel in each direction. The A-O modulator focusing lenses, blocking aperture, and in systems two and three (Figures 24 and 25) the transmit beam elevator and receive/LO splitter are mounted on holders with motion in one direction up to ½ inch with micrometer adjustment.

B. FIRST OPTICAL SYSTEM

The configuration of the first system developed to be utilized as a laser radar is shown in Figure 23. The transmit path was from the CO_2 laser reflected from the 95/5 beam

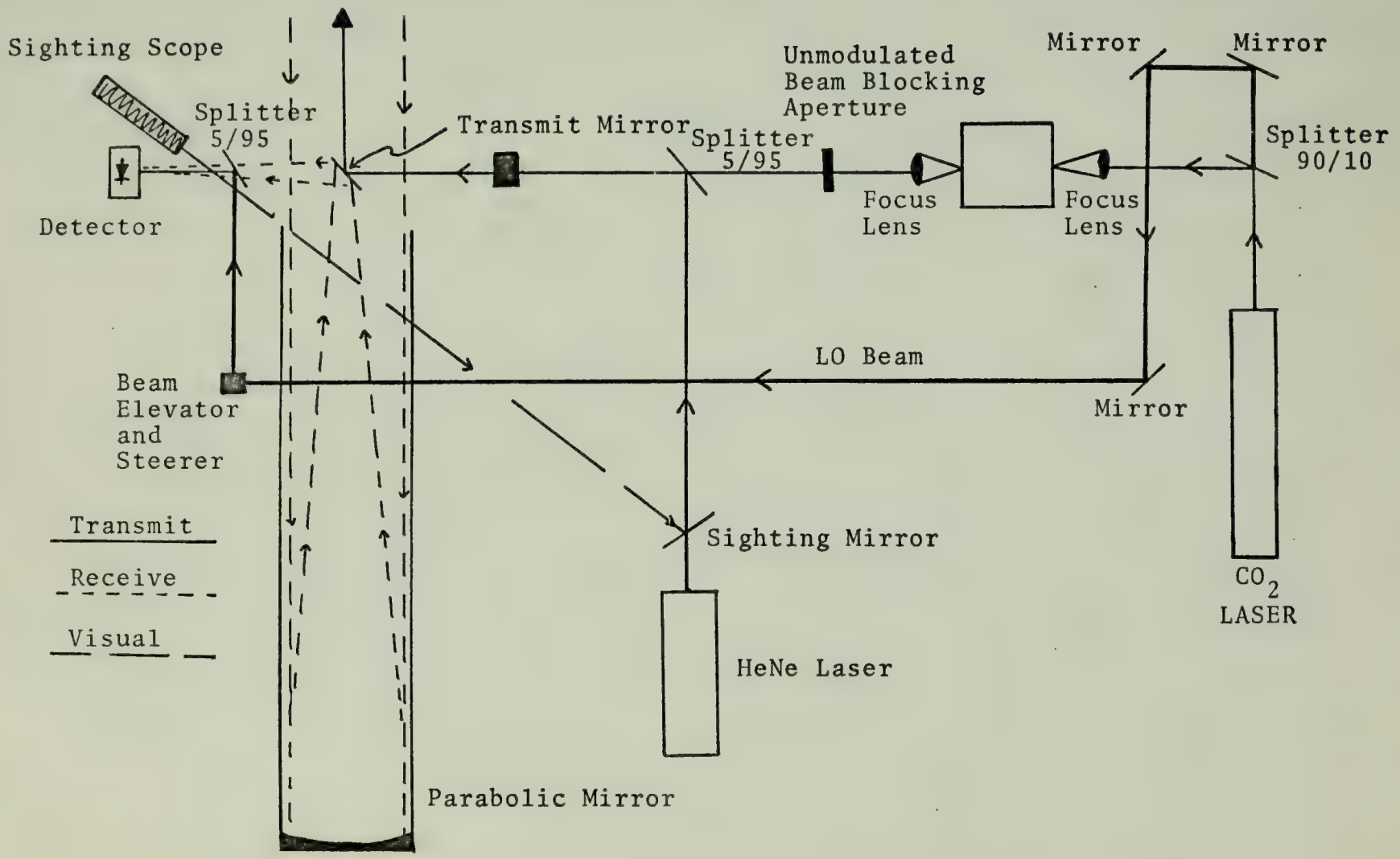

Figure 24. Second Optical System.

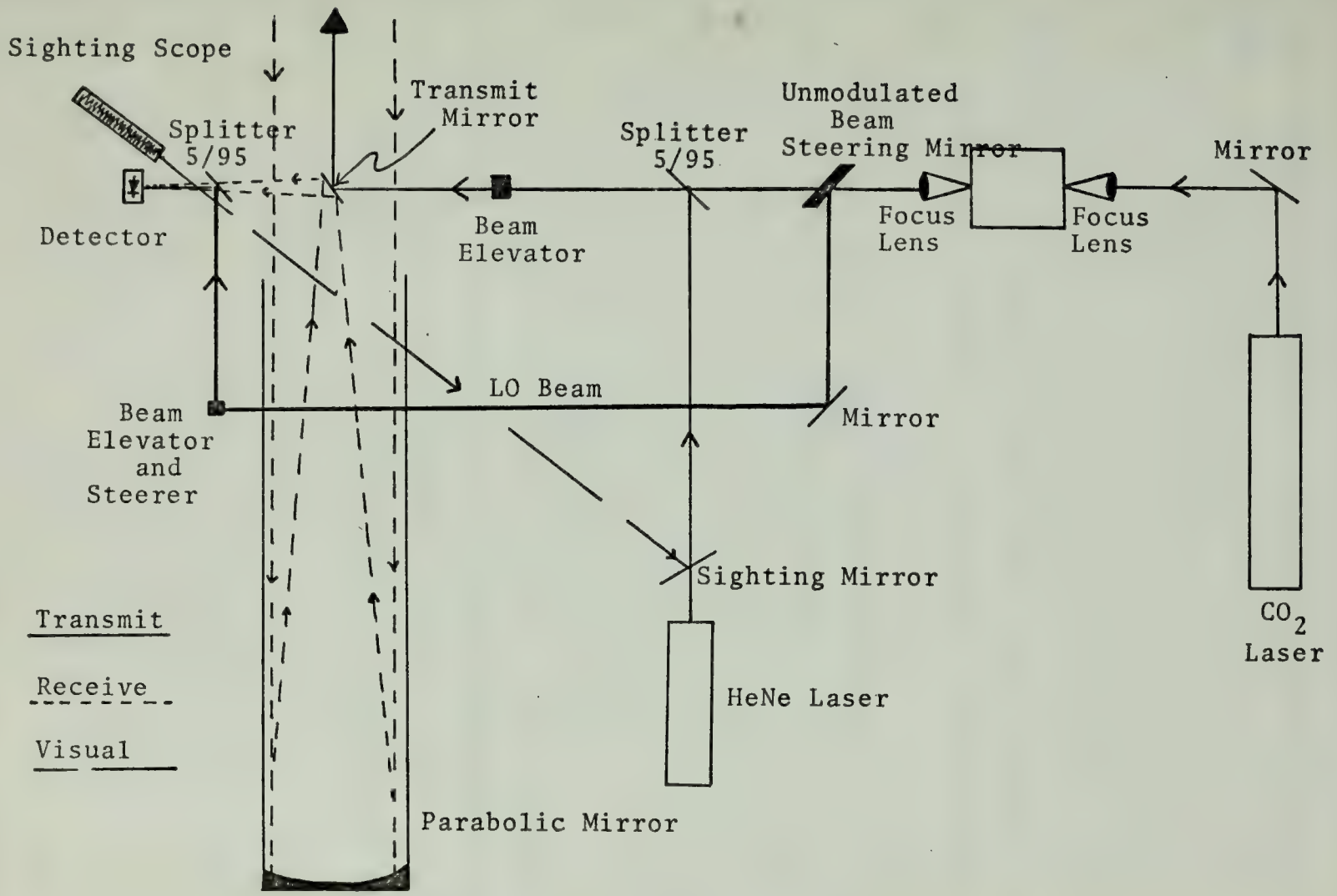

Figure 25. Third Optical System.

splitter (5% power losses) to the input focusing lens of the acousto-optic modulator, through the modulator to the output focusing/collimation lens, through the modulation pass aperture where the unmodulated portion of the beam is blocked, through the 50/50 splitter where half the power is reflected out of the system, through the 5/95 splitter (5% power loss) where the HeNe beam is collimated with the CO_2 transmit beam and off of the transmit/receive mirror to the target.

The return signal after being reflected from the target, enters the system at the transmit/receive mirror, through the 5/95 splitter (5% power loss), reflected off of the 50/50 splitter (50% power loss), through the 5/95 splitter (5% power loss) where the local oscillator beam is brought in, through the focusing lens to the detector.

The local oscillator path is from the laser through the 95/5 splitter (95% power loss), off three folding mirrors, reflected off of the 5/95 splitter (95% power loss) where it is combined with the return signal, through the focusing lens to the detector.

In the transmit path approximately 50% of the power into the A-O modulator is absorbed by the modulator and approximately 45% of the output is unmodulated and blocked. Of the remaining transmit power 50% is lost in the 50/50 splitter and another 5% is lost in the 5/95 splitter. Using these numbers, if 1 watt is transmitted from the laser approximately 124 mw is transmitted. In the LO path of 50 mw through the 95/5 splitter approximately 2.5 mw is focused on the detector.

The return signal is reduced to 45% of the original power by the splitters and to .707 of that by the aperture blockage mentioned in the previous section, for a net return on the detector of approximately 32% of the incoming power. In this manner the signal power out of the A-O modulator is reduced by 3.2 db in the transmit path and by 4.9 db in the return path for a net ideal optics loss of 8.1 db.

C. SECOND OPTICAL SYSTEM

The optical configuration of the second system utilized is shown in Figure 24. The important difference is the utilization of a Newtonian lens system as a transmit/receive antenna and using an unfocused local oscillator beam. The transmission, receive and local oscillator paths are shown in Figure 24. For the same 1 watt output from the laser approximately 235 mw is transmitted for a transmit gain of 2.8 db over system one.

The receive aperture of the second system is the 6 inch parabolic mirror of the Newtonian optics. The aperture area of the 6 inch mirror is nine times that of the 2 inch mirror less the elliptical mirror blockage of approximately 7% for a net 8.37 fold increase which is a 9.2 db gain due to aperture size alone. The loss due to one 5/95 splitter, the 50/50 splitter and due to the elliptical presentation of the angled splitters is eliminated for another 4.7 db gain. This nets a total gain in signal power of 16.7 db.

The utilization of an unfocused local oscillator beam instead of a focused beam greatly reduces the difficulty in

aligning the return signal and LO beam. It also provides a safety factor in the event the LO power should increase without operator knowledge because only a small portion of the increased power would fall on the detector. The adverse effect of using an unfocused LO beam is that it becomes much more difficult to provide enough local oscillator power incident upon the detector to achieve shot noise limited operation. Shot noise limited operation was not achieved in any of the three configurations.

D. THIRD OPTICAL SYSTEM

The third and final configuration is shown in Figure 25. The differences between system two and three are the replacement of the 90/10 splitter at the output of the laser by a mirror and the unmodulated output of the modulator is utilized as the LO beam. This provides a 10% increase in output power (.46 db) and a total LO power available of 510 mw as compared to approximately 230 mw.

E. ALIGNMENT TECHNIQUES

The alignment of the optical system is extremely critical. Because of the strict requirements a detailed description of the alignment procedure is presented.

1. Height Adjustments

All beams must move in a path parallel to the plane of the optical table to provide optimum alignment. To achieve this beam, height is measured at the output of an optical device and measured again at a distance as far away on the table as possible. If the heights are not the same

shims are introduced to adjust height or axis adjustments are made. As an example, the height of the laser beam at the laser output was measured. The first beam splitter was then adjusted so the beam was the same height at the opposite end of the table. The horizontal axis was adjusted so the beam was changed in direction by 90°.

2. Acousto-Optic Modulator Alignment

The CO_2 beam is focused into the germanium crystal in the modulator through a germanium focusing lens with a five inch focal length. The height of the lens was adjusted by shims until the CO_2 beam passed through the lens center. The modulator was mounted on a holder which would be adjusted with a micrometer setting so the angle of modulator axis could be adjusted with respect to the plane of the optical table. The modulator and holder were both mounted to one of the holders which are adjustable in three axes. The modulator was then positioned so the input beam passed through the center of the input aperture at a distance of five inches from the modulator center to the focusing lens so the beam waist would be in the center of the crystal. By using a level, the modulator was rotated until its axis was approximately two degrees from the vertical and then slowly adjusted until the output beam split into two beams. The positioning of the modulator was adjusted for maximum power in the modulated beam.

The recollimation lens was positioned in the two output beams five inches from the modulator center at a height where the two beams passed through near the lens

center. The recollimation lens serves a dual purpose in that it prevents a further divergence of the beams after their focal point and it collimates the beams so the modulated beam (which was deflected down at twice the Bragg angle) travels parallel to the plane of the table.

3. Collimation of the HeNe and CO_2 Transmit Beams

A visible beam from a HeNe laser was transmitted with the CO_2 beam to provide a visual indication of the location of the CO_2 beam. The HeNe beam entered the transmit path by reflecting off of the 5/95 beam splitter just prior to transmission from the system. Since the germanium splitter is opaque to visible light virtually all of the HeNe beam is transmitted.

For the HeNe beam to be collimated exactly with the CO_2 beam it must be positioned on the face of the 5/95 splitter at the exact position that the CO_2 beam passes through the splitter. The superpositioning can be determined by pressing a piece of liquid crystal paper on the face of the splitter. The intensity of the CO_2 beam is reduced by passing it through an aperture prior to the modulator. Care must be taken to position the aperture so the beam goes through the exact center so that the HeNe is positioned on the high intensity center of the beam. The HeNe beam can be adjusted in height by placing shims under the laser and horizontal adjustment is accomplished by rotating the laser slightly in the holder.

The HeNe transmit beam can be adjusted with the axis adjustments on the holder in which the splitter is

mounted. This adjustment does not effect the direction of the CO_2 beam transmission. A piece of heat sensitive graph paper was placed in the CO_2 beam approximately ten feet from the output, as soon as the graph paper began to darken the CO_2 beam was blocked and the HeNe beam was positioned on the small darkened spot. In this manner the HeNe beam can be positioned in the highest intensity portion of the CO_2 beam. The alignment was checked by passing both beams through an aperture onto a piece of liquid crystal paper located about forty feet from the output and about thirty feet from the aperture. If the beams are not collimated they will not be coincident at both the aperture and liquid crystal paper. Again care must be taken to position the aperture so the beams pass through its exact center or the beams on the liquid crystal paper may appear to be slightly misaligned when they are not. This appearance can be caused by passing parts of the CO_2 beam with a significant difference in power density. The difference in intensity will show on the liquid crystal and may give an appearance of misalignment.

A final alignment check was made approximately 305 yards from the output, on the roof of Ingersoll Hall. The dimension and location of the CO_2 beam was determined by chopping the transmit beam and reading the chopped output with a PbSnTe detector whose output was amplified 40 db and displayed on an oscilloscope. In the final alignment adjustment at this range the HeNe beam was lowered two inches

and moved horizontally one half inch. This movement was less than the divergence of either beam.

4. Collimation of Visual Optics with the CO_2 Transmit Beam

A visual sighting capability was incorporated into the system to enable placement of the transmit beam on a desired position. This is accomplished by utilizing a rifle sighting scope and a mirror with a hole in its center. The visual system is shown in Figures 23, 24 and 25.

The sighting mirror is positioned so the beam from the HeNe laser passes through the hole in its center. The rifle scope is then positioned so it looks onto the surface of the sighting mirror. The mirror is rotated until the rifle scope is sighting along the HeNe path. Initial alignment is facilitated by placing a mirror in the HeNe transmission path and adjusting it so the HeNe beam is folded back onto itself. The sighting mirror is adjusted properly when the HeNe beam reflects back through the rifle scope. Visual alignment is completed by adjusting the scope cross hairs on the bright return from a retro-reflector placed in the HeNe beam on the roof of Ingersoll Hall. Once alignment is completed the transmit beam can be positioned by sighting through the rifle scope and adjusting the optical table until the cross-hairs are positioned on the desired location.

5. Alignment of the Newtonian Optics

Alignment of the Newtonian transmit/receive optics is very critical since the theoretical field of view is only 127 μrad for an eight mil diameter detector (measured field of view was 180 μrad). Once the receive optics are aligned

with the transmit beam the detector is positioned at the focal point of the lens system. If the target is then moved out of the field of view but is still in the beam (which is much larger than the receive field of view) the focused energy moves off of the detector. At this point if the detector is repositioned in the received focused beam the signal can be processed as before. This demonstrates that there is a direct interaction between receive alignment and detector size and positioning.

By removing the 5/95 beam splitter which is positioned between the folding elliptical mirror and the detector (Figure 25) and placing a folding mirror in front of the detector the view of the receive optics can be determined. Looking back into the receive optics the blockage of the elliptical flat can be seen. When the HeNe beam is positioned on a retro-reflector located on the roof of Ingersoll Hall the red reflection can be faintly seen through the blockage image. This reflection is positioned in the center of the blockage by adjusting positioning screws on the back of the six inch parabolic mirror. The positioning can also be checked by moving horizontally and vertically and adjusting the parabolic mirror until the reflection bisects the blockage both vertically and horizontally.

Once the receive and transmit optics are aligned the return visible energy from the HeNe laser can be located by placing a white paper at the focal length of the optics (60 inches from the parabolic mirror). If the paper is moved slightly forward of the focal point the pattern of

the returned HeNe beam with its dark spot in the center (caused by the elliptical mirror blockage) can be seen. If the receive optics are properly aligned at this point the received pattern will be distorted by moving a paper in from the sides and top and bottom in front of the parabolic mirror. If the received pattern distorts as soon as the paper moves in front of the mirror from all sides then the Newtonian optics are aligned properly.

6. Signal and Local Oscillator Beam Alignment

The signal beam and local oscillator beam phase fronts must be aligned upon the detector surface nearly exactly. The local oscillator beam is unfocused to facilitate this alignment. While one beam was being aligned the other beam was blocked and vice versa.

With the 5/95 beam splitter removed as in the previous section, the HeNe return can be seen and the detector dewar can be positioned so the detector is very near the return signal. The CO_2 beam was then chopped by a fan and the detector position was varied in a raster type scan until the chopped output, amplified by 40 db, was seen on the oscilloscope. The 5/95 beam splitter was then repositioned in the signal and local oscillator path (oriented at approximately 45° with respect to each path). The beam splitter shifts the signal beam slightly and the detector was repositioned in the beam. After the detector was again positioned in the signal beam for maximum chopped signal amplitude the local oscillator beam was unblocked and the transmit beam was blocked. The local oscillator beam was

swept across the dewar aperture face in a raster pattern until the chopped output of the detector was maximized. After the detector was properly positioned and the rest of the system was aligned, the alignment is maintained and is correct as the table is repositioned to illuminate different targets.

F. ELECTRONICS AND SIGNAL PROCESSING

The block diagram of the signal processing system is shown in Figure 26. The system will be first analyzed considering a constant frequency IF of 30 MHz.

The driver for the acousto-optic modulator consists of a voltage controlled oscillator and a power amplifier. The output is coupled to the modulator with a tri-axial lead which minimizes RFI. Some of the output power was reflected back to the input terminal at a greatly reduced level. This reflected power provided a convenient means of obtaining the instantaneous transmitted frequency for comparison with the instantaneous received frequency for determination of the range and velocity frequency. The reflected reference signal is amplitude modulated by the input modulating signal which is a DC bias with a superimposed triangular modulating voltage. The reflected reference signal is passed through a high pass filter which eliminated the 1.75 kHz modulating waveform.

The transmit signal was connected to the R terminal of a balanced mixer. A 30 MHz reference signal of 1 volt amplitude (this amplitude was very critical for proper

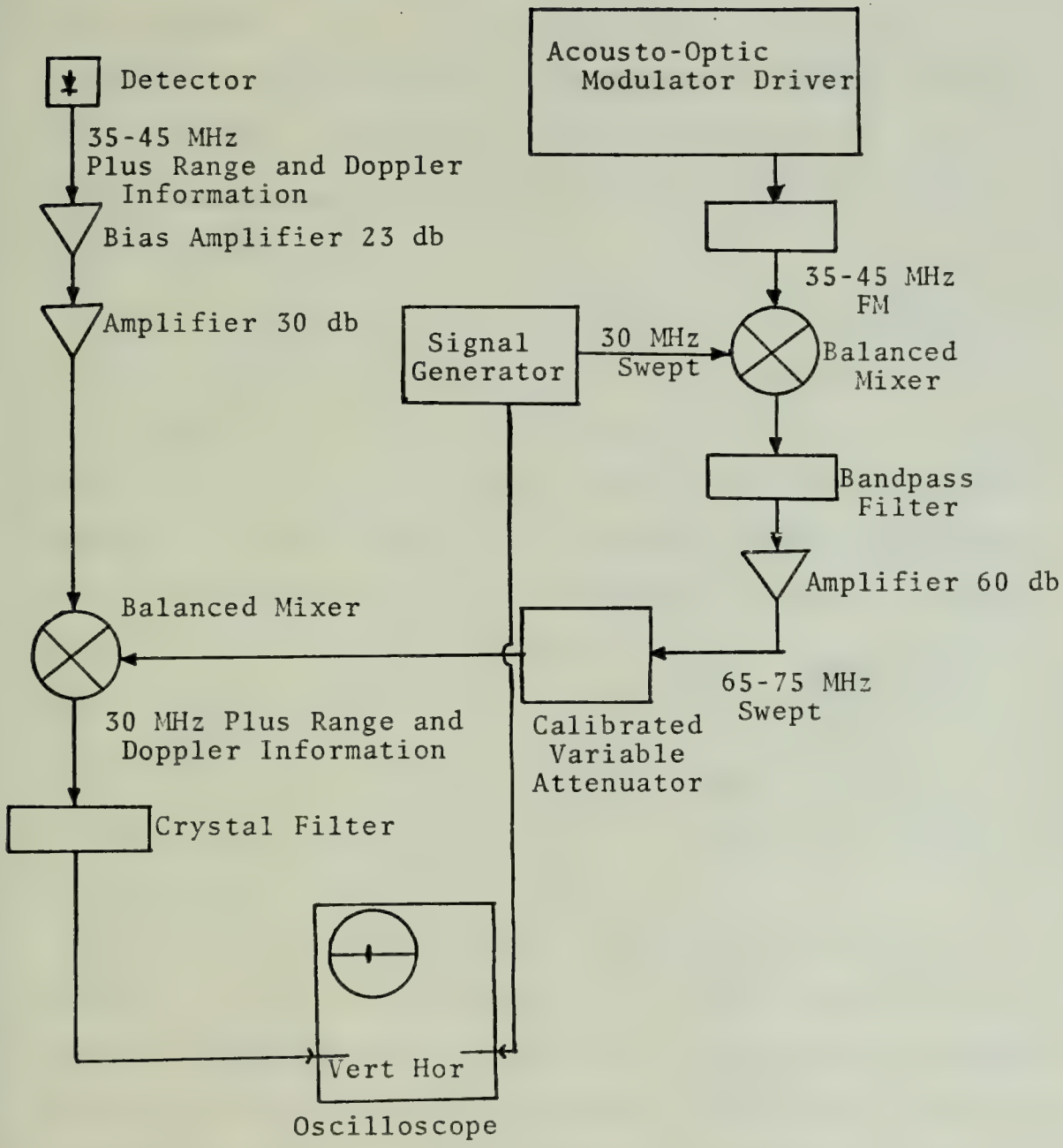

Figure 26. Signal Processing System.

operation of the balanced mixer) was connected to the L terminal. Both the sum and difference frequencies are present at the output of the mixer. This output was passed through a third order Butterworth filter with a bandpass of 60 - 80 MHz.

The 65 - 75 MHz signal was amplified 60 db and then attenuated 8 db (to obtain the one volt necessary for the balanced mixer) and connected to the L input of the second balanced mixer.

The output of the PbSnTe Detector is a 35 - 45 MHz signal offset by any doppler shift which may be present. This signal is amplified by a 23 db bias amplifier with a 3 db noise figure and then by a 30 db amplifier. This signal is then connected to the R input of the second balanced mixer where it is mixed with the 65 - 75 MHz reference signal. The output of the second mixer is 30 MHz + F_{range} + $F_{doppler}$ and a 100 - 120 MHz spread. The range information is present at the output as a signal at 30 MHz + F_{range} and 30 MHz - F_{range}. The double frequency spikes are present because of the triangular frequency modulation.

The output frequencies were observed in a spectrum analyzer. If the 30 MHz output of the signal generator into the first balanced mixer is varied the output range frequencies are varied in the same way. In this way the range frequencies were swept across a 3.5 kHz crystal filter centered at 30 MHz. As the range frequencies were swept across the filter bandwidth the signals were connected to the vertical input of an oscilloscope. The input to the horizontal grids of

the oscilloscope was the sweep output from the sweeping signal generator and in this way the horizontal sweep was calibrated to the frequency sweeping of the return signal. The resultant output of this processing was an A scope range presentation on the oscilloscope. The A scope presentation was not very satisfactory because of the frequency output of the signal generator drifted making a range displacement calibration impossible. Other than a demonstration of its feasibility the A scope presentation was not utilized. The range and velocity information was determined directly from the spectrum analyzer.

G. SYSTEM RADAR ANALYSIS

The theoretical development for a FM-CW radar is presented in Chapter II section A. The specific system parameters are as follows:

Carrier frequency	$f_o = 2.83 \times 10^{13}$ Hz
Wavelength	$\lambda = 10.6$ μm
Resolution filter bandwidth	BW = 3.5 kHz centered at 30 MHz
Triangular wave modulation frequency	FM = 1.75 Hz
Total frequency deviation	$2\Delta F$ = 10 MHz centered at 40 MHz

These parameters yield the following system performance capabilities

df/dt (equation 3)	3.5×10^{10} Hz/sec
Unambiguous range (equation 19)	42.9 km
Range frequency (equation 5)	233.3 kHz/km 213.3 kHz/100 yds

Velocity frequency (equation 13)	52.4 kHz/km/hr 97 kHz/knot
Range resolution (equation 21)	15 m
Velocity resolution (equation 22)	.036 knots
Acceleration spectrum spread tolerance (equation 17)	6.6 g

V. EXPERIMENTAL PROCEDURES AND RESULTS

A. DETERMINATION OF RANGE

For an initial determination of the practicability of determining range by the expected range frequency signals the first system (Figure 23) was used. The output power was reduced and attenuated until only a few milliwatts were transmitted. The output beam was folded around the room and out along the top of the sixth floor of Spannagel Hall. A front-surfaced mirror was placed at several known distances and the range frequency was determined and compared with the expected frequency shift. It was during this operation that the offset from zero range was first noticed (explained in Chapter III, Section B). Table V contains the results of this series of experiments. It should be noted that the results agree well within the accuracy of the frequency readings. Figure 27 is a photograph of the first system configuration.

An unexpected phenomenon was the appearance of a zero range beat frequency. This is believed to be caused by a reflection of some of the modulated beam from the output face of the modulator crystal back into the laser. Once in the laser, the modulated frequency is amplified and transmitted along with the normal unmodulated frequency and in this manner it is introduced into the local oscillator beam. It was determined to be in the local oscillator path because it remained even when the output beam was blocked.

Table V. Range Frequency Determination as a Function of Range.

Triangular Modulation F_m = 10 kHz
$2\Delta F$ = 10 MHz $df/dt = 2 \times 10^{11}$ Hz/sec
Range Frequency Shift = 1.22 kHz/rd
Spectrum Analyzer Dispersion 50 kHz/cm

Range	43 ft	Expected Range Frequency	17.5 kHz
		Actual Range Frequency	345 kHz
		Frequency Offset	327.5 kHz
		Corresponding Offset Time Delay	1.64 μsec
Range	67 ft	Expected Range Frequency	27.2 kHz
		Actual Range Frequency	360 kHz
		Frequency Offset	332.8 kHz
		Corresponding Offset Time Delay	1.66 μsec
Range	91 ft	Expected Range Frequency	37 kHz
		Actual Range Frequency	367 kHz
		Frequency Offset	330 kHz
		Corresponding Offset Time Delay	1.65 μsec
Range	115 ft	Expected Range Frequency	46.8 kHz
		Actual Range Frequency	375 kHz
		Frequency Offset	328.2 kHz
		Corresponding Offset Time Delay	1.64 μsec
Range	139 ft	Expected Range Frequency	46.3 kHz
		Actual Range Frequency	387.5 kHz
		Frequency Offset	341.2 kHz
		Corresponding Offset Time Delay	1.7 μsec
Range	163 ft	Expected Range Frequency	66.3 kHz
		Actual Range Frequency	395 kHz
		Frequency Offset	328.7 kHz
		Corresponding Offset Time Delay	1.64 μsec
Range	187 ft	Expected Range Frequency	76 kHz
		Actual Range Frequency	405 kHz
		Frequency Offset	329 kHz
		Corresponding Offset Time Delay	1.64 μsec
Range	211 ft	Expected Range Frequency	85.8 kHz
		Actual Range Frequency	415 kHz
		Frequency Offset	329.2 kHz
		Corresponding Offset Time Delay	1.64 μsec

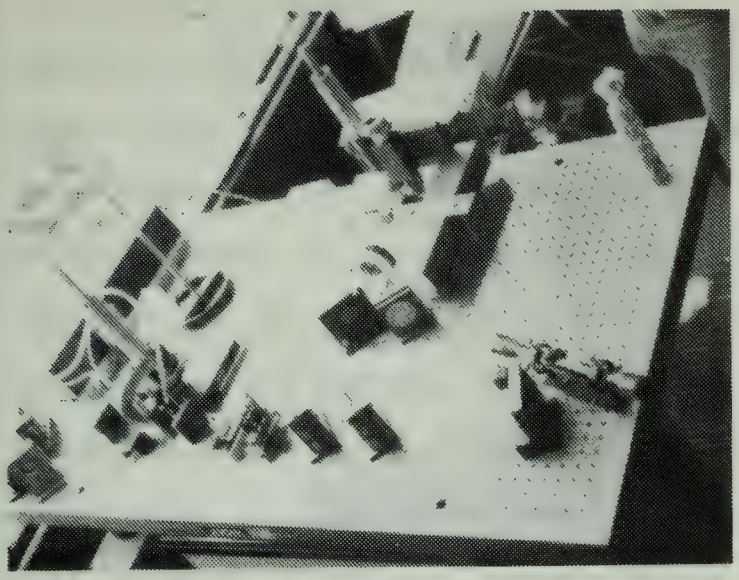

Figure 27. First Optical System.

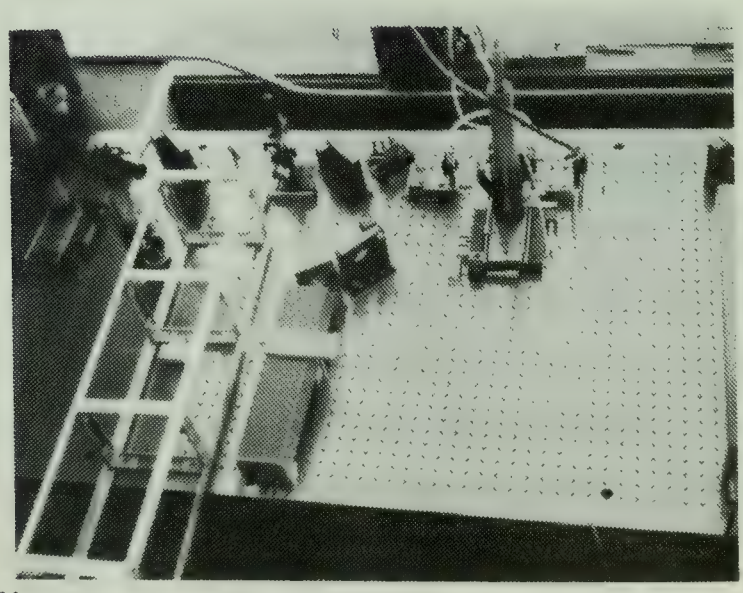

Figure 28. Third Optical System, View 1.

The zero range frequency is believed to be due to internal laser amplification rather than a reflection from the output mirror because of the marked variation of the amplitude of the signal at different times. The signal on the LO path was first noticed at NELC during the experience tour in San Diego. Prior to bringing the laser to NPS it was recharged and for the first couple of weeks of operation at NPS the signal was not present on the LO beam. At other times the signal was not present when the laser was first turned on but became present after the laser had warmed up. The signal strength fluctuated from week to week and for the last several weeks was significantly lower than at other times. All of these variations can logically be reasoned to be due to the effects of pressure and temperature line broadening and due to the variations in line width of various laser transmission lines.

B. TARGET DETERMINATION AT 305 YARDS

The next step in system development was to determine the system capability at a greater distance. For this work, the system configuration of the second system (Figure 24) was initially used and finally that of the third system (Figure 25). Figures 28 and 29 are photographs of the third system. Figure 30 shows the view from Spannagel 704 to the top of Ingersoll Hall and Figure 31 shows the NPS grounds.

During this and subsequent experimental stages the target was a two-inch diameter, gold surfaced retro-reflector. The retro-reflector is shown mounted on a model railroad car

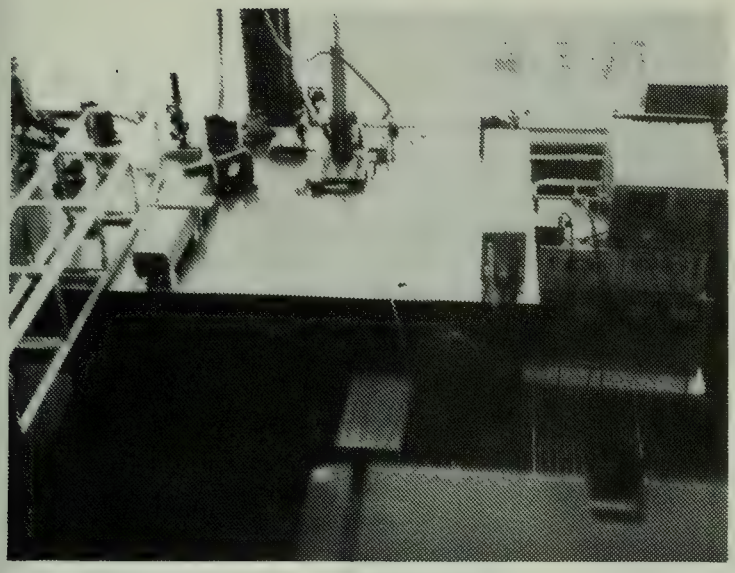

Figure 29. Third Optical System.

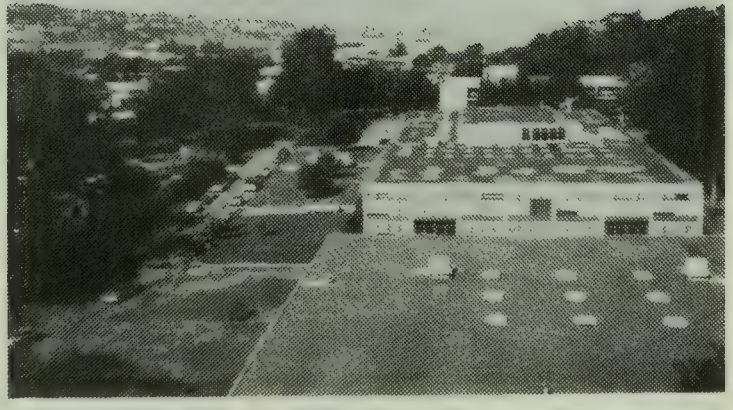

Figure 30. View from Spanagall Hall to Ingersoll Hall.

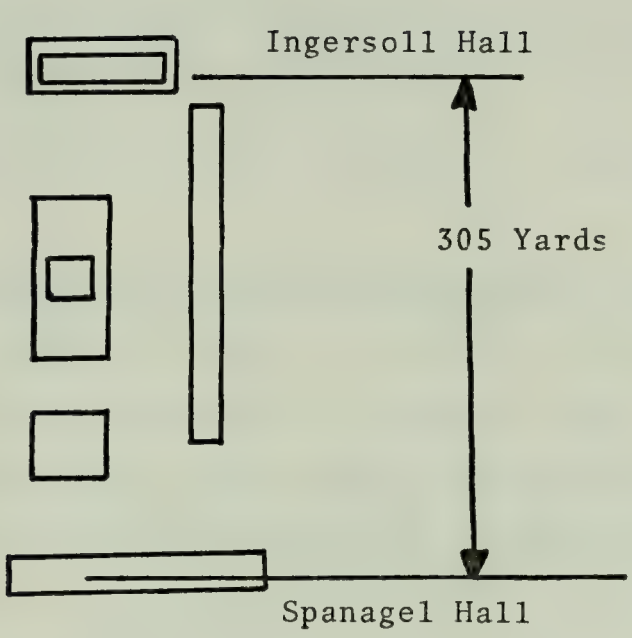

Figure 31. Naval Postgraduate Grounds, Near Range Target.

in the photographs of Figures 32 and 33. The retro-reflector is diffraction limited at 10.6 μm and the reflected energy from it has the same divergence as the incident beam.

The modulator was readjusted between the experiments of Section A and determining the target on Ingersoll. At the new height position, the time delay was approximately 1 μsec which for the 1.75 kHz modulation rate corresponds at a 35 kHz frequency offset. Figure 34 shows the zero range frequency signal. The small spikes offset about 35 kHz from the center in Figure 36 and are the zero range frequencies along with the signal from the retro-reflector. In both photographs the spectrum analyzer dispersion was 50 kHz/cm.

1. Return Signal from Retro-Reflector at 305 Yards

The system was aimed at the retro-reflector on Ingersoll Hall and optimized for maximum signal. Figure 35 shows the unprocessed return out of the detector and Figures 36 and 37 show the processed return. The following conditions existed:

Transmit Frequency	35 - 45 MHz
Modulating Rate	1.75 kHz
Target Range	305 yards
Analyzer Dispersion and Noise Bandwidth	
For Total Spectrum	2 MHz/cm
For Range Frequency	50 kHz/cm
df/dt	3.5×10^{10} Hz/sec

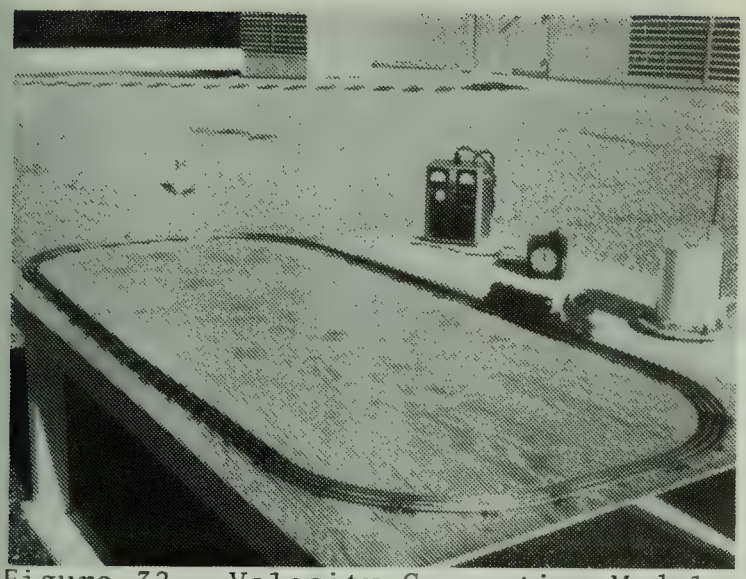

Figure 32. Velocity Generating Model Railroad, View 1.

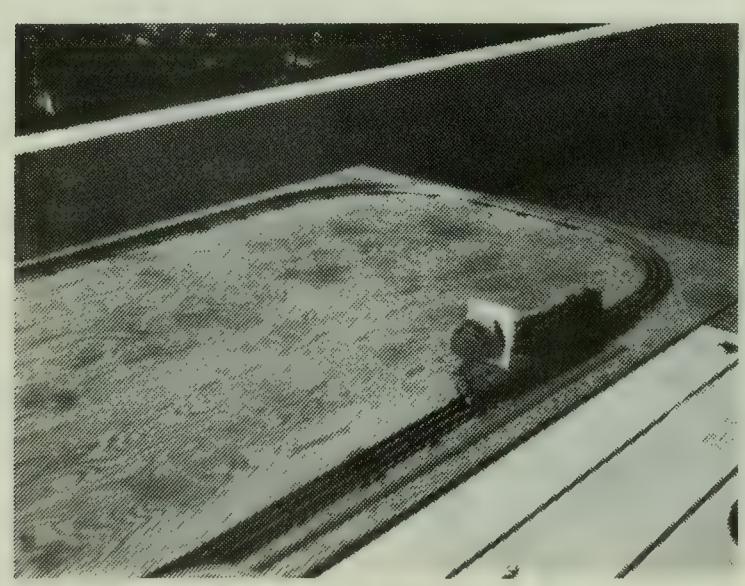

Figure 33. Velocity Generating Model Railroad, View 2.

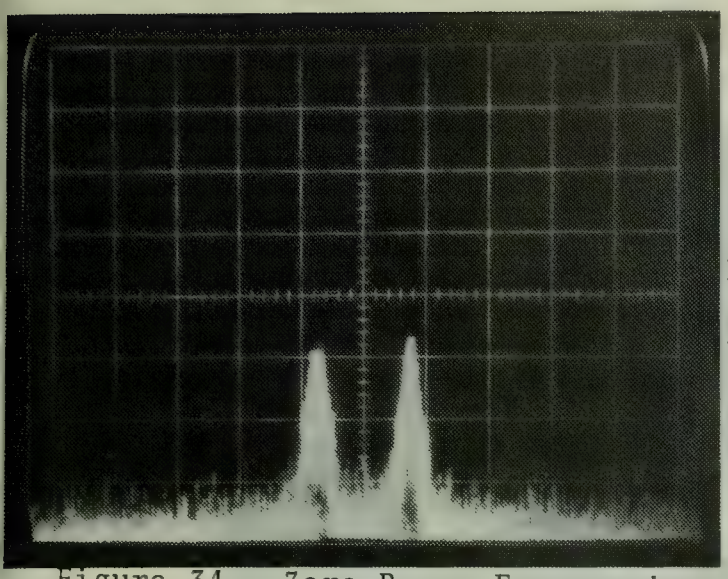

Dispersion 50 KHz/cm

Frequency Offset ≈ 35 kHz

Figure 34. Zero Range Frequencies.

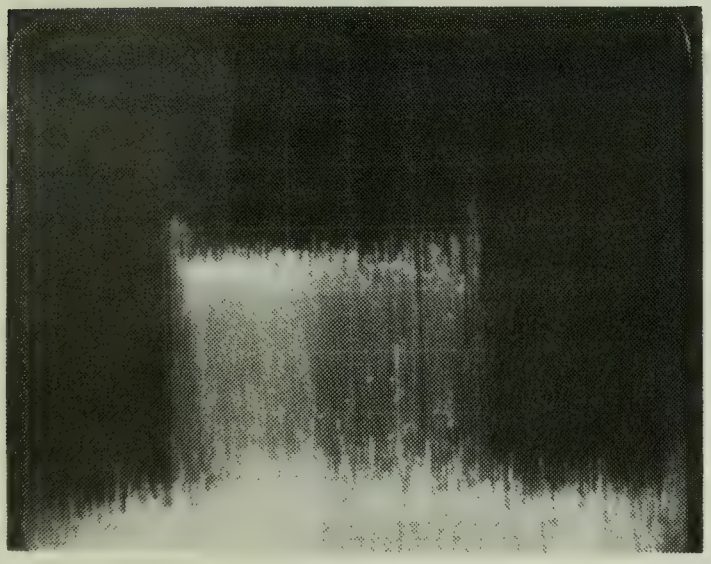

Dispersion 2 MHz/cm

S/N 50 db

Total Spectrum 10 MHz

Figure 35. Unprocessed Detector Output for 305 Yard Target.

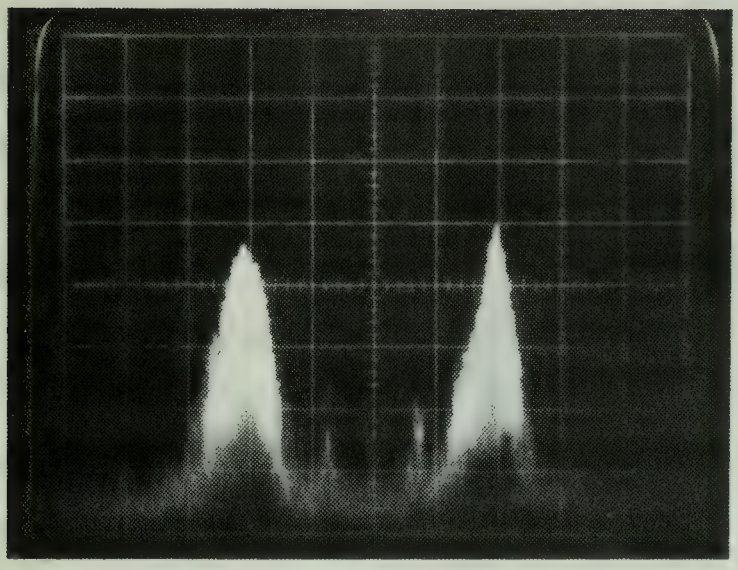

Dispersion	50 kHz/cm
Total Separation	200 kHz/cm
Zero Range Frequencies	± 35 kHz
305 Yard Range Frequencies	± 100 kHz
Range Frequencies	± 65 kHz
Expected Frequencies	± 65.1 kHz

Figure 36. Processed Return for 305 Yard Target.

The following are the resultant data:

Total Spectrum S/N	55 db
Range Frequency S/N	60 db
Zero Range Frequency	±35 kHz
Time Offset	1 μsec
Range Frequency (including zero range)	±100 kHz
Actual Range Frequency	65 kHz
Expected Range Frequency	65.1 kHz
Transmitted Power	.65 w
LO Unfocused Power	.51 w
Chopped Signal Output	5.5 mv
Chopped LO Output	1.4 mv
Returned Signal Power	.75 mw

(Prior to the 5/95 splitter)

The range frequency results agreed almost exactly with those expected. The noise bandwidth of the processed signal was 16 db narrower than the total spectrum bandwidth. There was a 5 db S/N gain and there was a 6 db insertion loss at the input of the balanced mixer. The other 5 db could be accounted for by noise addition of the mixer.

2. Transmit Divergence Determination

With both the transmitted and returned power known and the target range known, the beam divergence can be calculated. The returned power was readily measured because the HeNe focused return was easily seen. The returned power was measured with the low-range (<200 mw) digital power meter while the transmit power was measured with the high-range meter. This is a possible source of error but all

calculations are based upon these readings being correct. The divergence calculations are made considering the reflecting and receive aperture areas as compared to the total area of an arc subtended by a beam of a known divergence at the known range. Since everything is known but the divergence, it can readily be determined.

The arc length of a beam of a given divergence at a given range is given by

$$d = R\theta \tag{65}$$

and its area is

$$\pi\left(\frac{d}{2}\right)^2 = \pi\left(\frac{R\theta}{2}\right)^2. \tag{66}$$

The area of the retro-reflector compared to this area is

$$\frac{\pi\left(\frac{D_t}{2}\right)^2}{\pi\left(\frac{R\theta}{2}\right)^2}. \tag{67}$$

The divergence from the return from the retro-reflector is the same as the incident beam. This results in an illuminated area at the receive aperture the same size as that at the target. The ratio of the received power to returned power is thus

$$\frac{\pi\left(\frac{D_r}{2}\right)^2}{\pi\left(\frac{R\theta}{2}\right)^2}. \tag{68}$$

The net return power is thus given by

$$P_r = \frac{P_t \pi^2 \left(\frac{D_t}{2}\right)^2 \left(\frac{D_r}{2}\right)^2}{\pi^2 \left(\frac{R\theta}{2}\right)^4} = \frac{P_t D_t^2 D_r^2}{(R\theta)^4} . \qquad (69)$$

In this situation the return power is known and thus the divergence can be determined from

$$\theta = \left(\frac{P_t}{P_r} \frac{D_t^2 D_r^2}{R^4} \right)^{\frac{1}{4}} \qquad (70)$$

$$\theta = \left(\frac{.65 \text{ w}}{.75 \text{ mw}} \cdot \frac{2^2 \text{in} \cdot 6^2 \text{in}}{(305 \text{ yd} \cdot 36 \text{ in/yd})^4} \right)^{\frac{1}{4}} = 1.71 \text{ mradian}$$

3. Field of View Measurement

The field of view of the receive optics was measured by placing the retro-reflector in the beam in a position where the return signal was maximum. The reflector was then moved a known amount and the signal strength was noted. The beam width was defined as the 3 db points of the signal decrease. The field of view was determined using equation (65).

The 3 db beam width was determined to be nearly symmetrical at 5 cm. At a range of 305 yards this gives a field of view of 179 μradian. This compares reasonably well to the theoretical far-field field of view of 127 μradian.

There are two effects not considered in this computation. The first is that the target range is not in the far field of the optics (305 yards vice 1199 yards). The effect of this is an enlargement of the Airy disc diameter

which reduces the theoretical field of view. Offsetting this is the effect of the finite reflector size (2 inches vice a point). The separation was measured from the reflector center so the reflector extended on both sides of this point. Since the beam intensity distribution should be nearly Gaussian this would tend to increase the apparent beam width.

4. Expected Return from a Diffuse Reflector at 305 Yards

The return from a diffuse target would greatly decrease the return signal received at the receive aperture. If one assumes an ideal Lambertian return [14] from a diffuse reflector, the area illuminated is that subtended by a solid angle of π radians. The resultant reflected energy would then be reflected over an area of

$$A = \pi R^2 \tag{71}$$

instead of

$$A = \pi\left(\frac{R\theta}{2}\right)^2. \tag{72}$$

The difference in area and thus power density is the square of the beam divergence. For a divergence of 1.71 mrad, this is a 61.3 db reduction of signal power. With a processed S/N of 60 db, it might be possible to see the return for an ideal diffuse reflector larger than the retro-reflector.

The target that was utilized for the diffuse target consisted of two 1-1/2" x 6" pieces of sandblasted aluminum placed side by side. The target had been exposed to air for several months so there was undoubetdly some surface

oxidation. Additionally, the assumption of a perfectly diffuse reflector was an approximation. The larger area of the diffuse reflector provided a gain in reflecting area at the target of approximately 7.6 db. The surface of the target caused attenuation of the incident power and a 6 db reflection loss as compared to an ideal Lambertian is not unreasonable. Using these numbers, the expected return of the diffuse reflector would be .3 db. No return signal was detected from the diffuse reflector even though the target was varied widely in angular presentation.

5. Calculation of Detector Quantum Efficiency

The quantum efficiency of a detector is that proportion of incident photons which are converted to a utilizable signal as compared to the total incident flux. The quantum efficiency of a photodiode can be calculated from the relationship [15]

$$\eta = \frac{hf_o v}{qPR} \tag{73}$$

where η is the quantum efficiency, f_o is the frequency of the incident photon, v is the detector output voltage, q is the electronic charge, P is the incident power and R is the zero bias detector resistance. The incident power is the power incident upon the detector. The Airy disc for a far field target is not in the far-field, the actual Airy disc is somewhat larger. The detector size is 200 μm so it is smaller than the Airy disc. The energy density profile of the Airy disc is shown in Figure 5.5 of [17]. Since the detector size is less than 74% of the Airy disc diameter,

it is estimated that approximately 80% of the power in the Airy disc is incident upon the detector. The power contained in the Airy disc is approximately 84% of the total focused power [17]. The dewar window transmittance is estimated at .8 which is reasonable for a good window. The total power incident at the dewar (after passing through the 5/95 beam splitter) was .7 mw. When all of the aforementioned effects are considered, the estimated power incident on the detector is .38 mw. Thus the quantum efficiency is given by

$$\eta = \frac{(6.63 \times 10^{-34})(2.83 \times 10^{13})(5.5 \times 10^{-3})}{(1.6 \times 10^{-19})(3.8 \times 10^{-4})} = .034.$$

As mentioned in Chapter III, Section C, this value is surprisingly low and tends to indicate that the detector has degraded. There are several possible sources of error in this calculation but the result is still nearly one order of magnitude below the expected value of .14.

6. Calculation of Noise Equivalent Power

Noise equivalent power id defined as the amount of power necessary for a signal-to-noise ratio of one with a unity noise bandwidth. This can be computed if the signal power, noise bandwidth and S/N are known. Using measured values and the same estimations utilized in the previous section, the computation is as follows:

Signal Power	$\simeq$ .38 mw
S/N	= 60 db
Noise bandwidth	= 50 kHz

$$NEP = \frac{B}{(S/N)B} = \frac{3.8 \times 10^{-4}}{10^{6 \cdot 5} \times 10^{4}} = 7.6 \times 10^{-15} \quad w/Hz$$

From equation (52), it can be seen that for shot noise limited operation

$$NEP = \frac{hf_o B}{\eta} . \tag{74}$$

For unity bandwidth and quantum efficiency

$$NEP_{ideal} = hf_o = (6.63 \times 10^{-34})(2.83 \times 10^{13}) = 1.88 \times 10^{-20} w$$

For a noise bandwidth of 50 kHz, this becomes 9.4×10^{-16} and for $\eta = .034$.

$$NEP = 2.76 \times 10^{-14} \text{ w.}$$

This value is larger than the computed value which indicates that either the noise bandwidth is incorrect, S/N is incorrect or the computed value of η is incorrect. The noise bandwidth is determined by the dispersion of the spectrum analyzer and the S/N ratio 60 db has been repeated several times. These factors indicate that the computed value of conversion efficiency is incorrect. For shot limited operation, this would correspond to a value for η of .12 which is near the tabulated value of approximately .32 (for a reverse bias of .17 v). Since shot noise limited operation was not obtained, this value is reasonable. The readings utilized for the computation of η in Section IV were reproduced several times also.

C. EXTENDED RANGE CAPABILITY

After successfully detecting the retro-reflector at 305 yards, an extension of target range was completed. There was a clear area at the edge of El Estero Lake at an unknown range. The retro-reflector was taken to this area and illuminated. The resultant signal had a S/N ratio of 35 db and a frequency shift of 260 kHz including the zero range shift of 35 kHz. The net frequency shift of 225 kHz corresponds to a range of 1055 yards. The range of 1055 yards is approximately 3-1/2 times as far as 305 yards. Since the signal strength decreases as R^{-4}, this should give a corresponding reduction in the S/N ratio of 21.5 db. The total range (both directions) is approximately 2 km so this would provide an additional attenuation of approximately 2 db. Thus the expected S/N ratio was 36.5 db which agrees very closely to the experimental value of 35 db.

The next step in range was to illuminate the retro-reflector while it was on the Coast Guard pier at a range of approximately 2400 yards (Figure 37). This is approximately eight times the range of Ingersoll Hall and again considering the R^{-4} signal relationship, this should cause a reduction of the S/N ratio of 36.1 db. The total range is slightly more than 4 km which would give an expected reduction in signal strength of 4 db due to attenuation. These considerations indicate an expected signal-to-noise ratio of 20 db and a frequency shift (including the zero

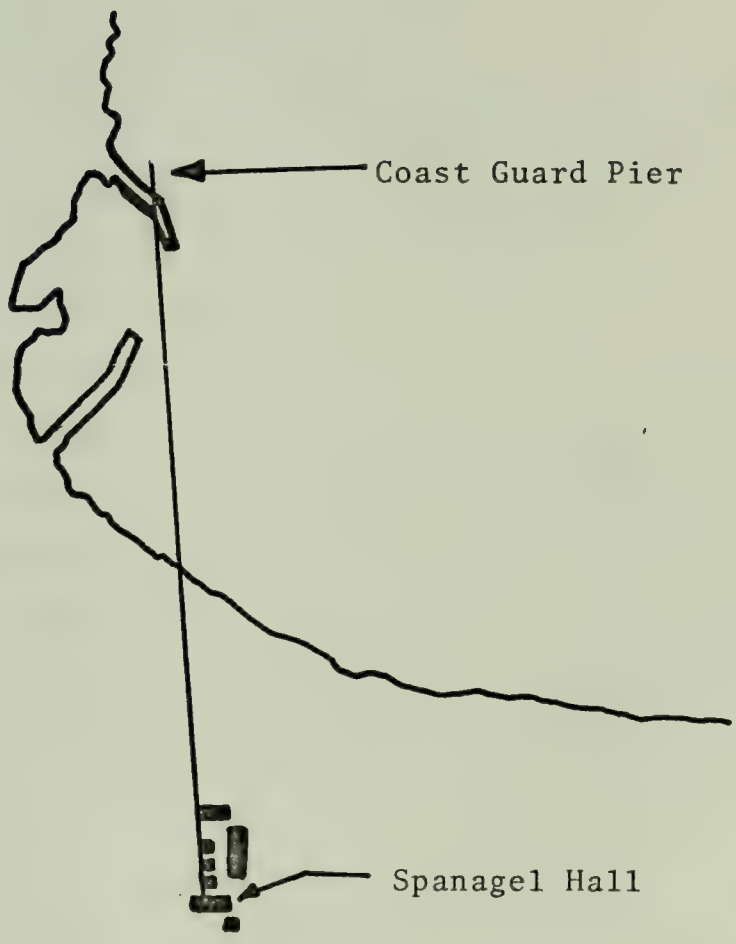

Figure 37. Far Range Target Measurement.

range shift) of 547 kHz. The experimentally determined values were:

S/N	20 db
Frequency Shift	540 kHz

This frequency shift indicates an actual range of 2370 yards. Figures 38 and 39 show the signal from the Coast Guard pier.

D. VELOCITY DETERMINATION

If a target with relative velocity is illuminated by the radar, the return should be shifted in frequency by the amount of 188.7 kHz/msec^{-1} relative velocity with the sign being the same as that of the relative velocity. To facilitate velocity measurements, a model train was set-up on the roof of Ingersoll so that the beam only illuminated one side of the oval track. A meter stick was positioned along a straight portion of the track and an electric timer was used to measure the amount of time the reflector was alongside the meter stick. Figures 32 and 33 show the experimental set-up for this measurement. Some problems were experienced with the electric timer switch and the train was not stable enough to obtain the desired velocity range. Additionally there are inherent errors which are unavoidable when manually timing. Doppler shifts of both senses were obtained by reversing the direction of the model train. Due to a difference in elevation there was a 5.5° angle between the velocity motion and the radar beam; because of this, the measured velocity must be

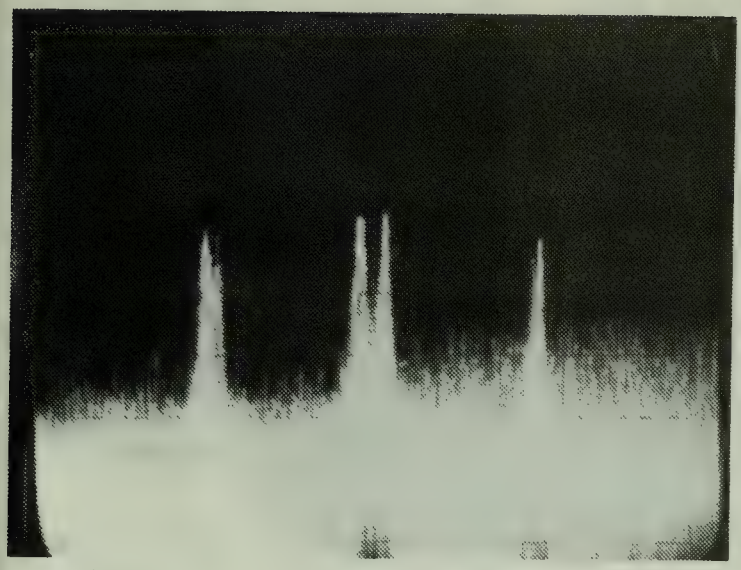

Dispersion	200 kHz/cm
Range	2370 yard
S/N	20 db
Zero Range	± 35 kHz
Range Frequencies	±505 kHz
Range Return	±540 kHz

Figure 38. Processed Return for 2379 Yard Target, View 1

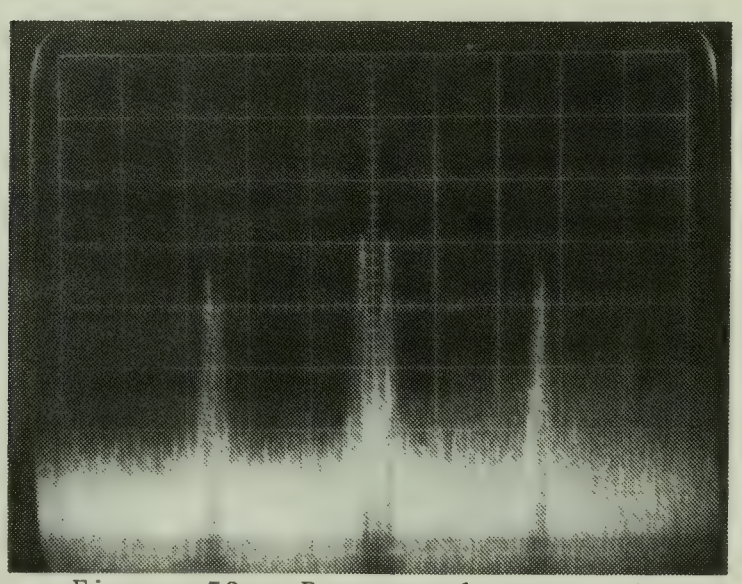

Dispersion	200 kHz/cm
Range	2370 yard
S/N	20 db
Zero Range	± 35 kHz
Range Frequencies	±505 kHz
Range Return	±540 kHz

Figure 39. Processed Return for 2370 Yard Target, View 2.

multiplied by cos 5.5° to obtain the velocity component relative to the radar. Four photographs are included of the doppler shift measurements; these are Figures 40, 41, 42 and 43. Table VI lists the results of the velocity measurements. The measured values were well within the tolerances of measurement error.

A totally unexpected phenomenon was noted during the velocity measurements. In addition to the expected doppler frequency shift, the range frequencies with no doppler shift were present at a much reduced signal strength. There was no return from the tracks until the train with the reflector moved into the beam. All parts of the train were, of course, moving at the same speed. Later the reflector was hand held and moved and again this phenomenon was observed. This zero velocity component should not have been present since any return reflection should have been doppler shifted.

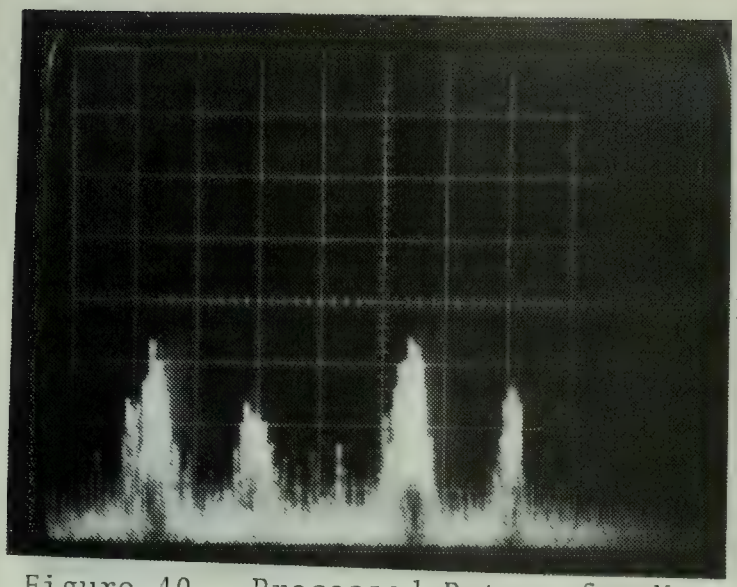

Dispersion 50 kHz/cm

Figure 40. Processed Return for Negative Relative Velocity, View 1.

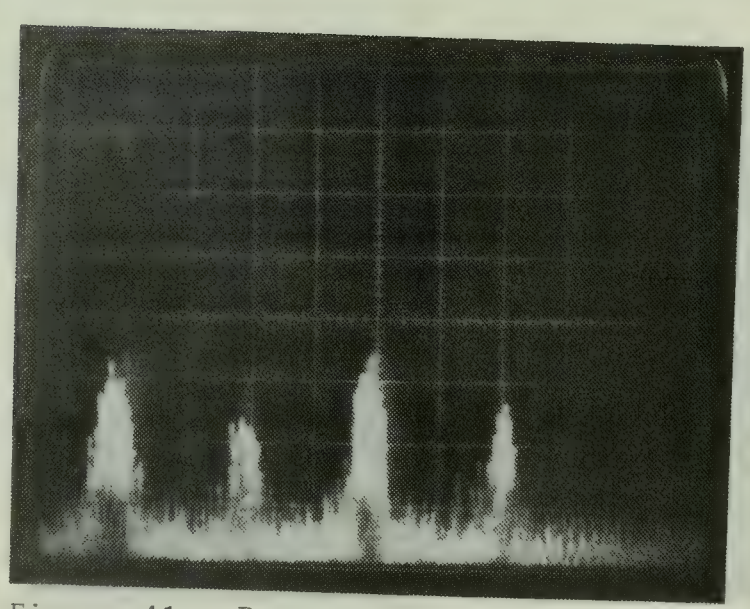

Dispersion 50 kHz/cm

Figure 41. Processed Return for Negative Relative Velocity, View 2.

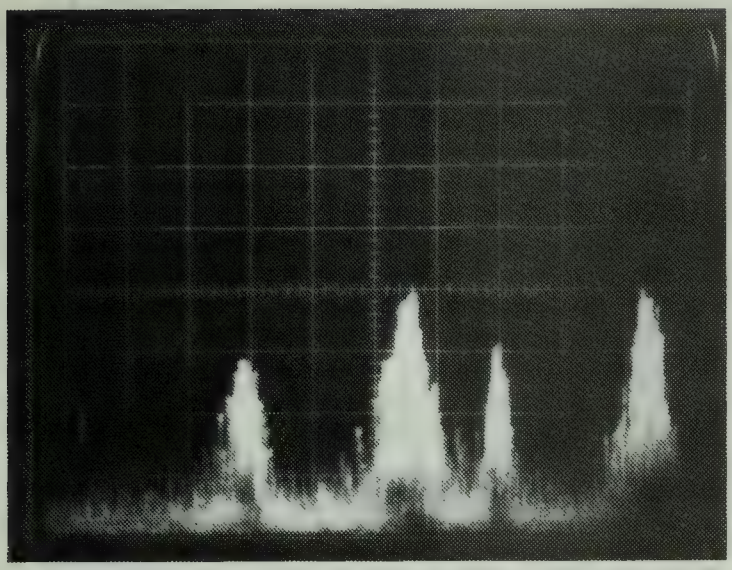

Dispersion 50 kHz/cm

Figure 42. Processed Return for Positive Relative Velocity, View 1.

Dispersion 50 kHz/cm

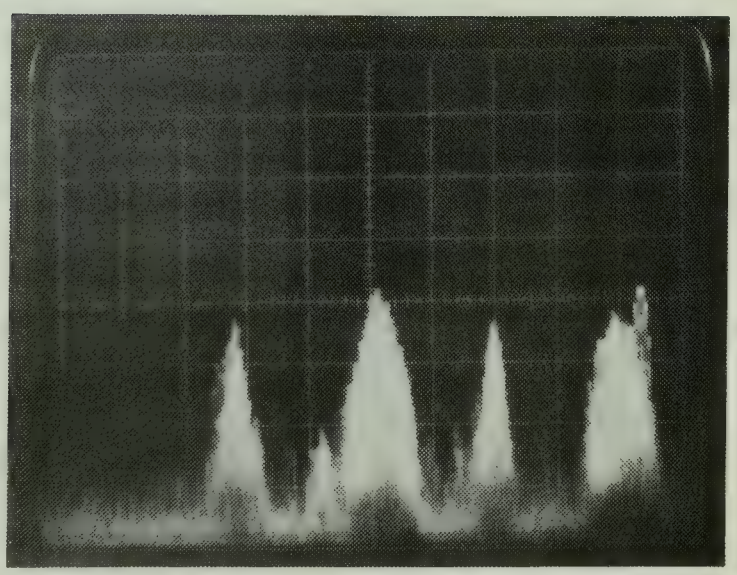

Figure 43. Processed Return for Positive Relative Velocity, View 2.

Figure 40	Down Doppler Shift
1/v	≈ 2.7 sec/m
v	≈ .37 m/sec
Expected Frequency Shift	69.5 kHz
Actual Frequency Shift	≈ 80 kHz
Figure 41	Down Doppler Shift
1/v	≈ 1.8 sec/m
v	≈ .56 m/sec
Expected Frequency Shift	104 kHz
Actual Frequency Shift	≈ 110 kHz
Figure 42	Up Doppler Shift
1/v	≈ 1.6 sec/m
v	≈ .63 m/sec
Expected Frequency Shift	117 kHz
Actual Frequency Shift	≈ 120 kHz
Figure 43	Up Doppler Shift
1/v	≈ 1.7 sec/m
v	≈ .59 m/sec
Expected Frequency Shift	110 kHz
Actual Frequency Shift	≈ 115 kHz

Table VI. Velocity Determination Results.

VI. CONCLUSIONS AND RECOMMENDATIONS

A. CONCLUSIONS

The experimental results obtained closely agreed with the theoretically expected results and prove the basic feasibility of constructing a FM-CW optical radar and frequency modulation and coherent detection of a laser beam. The capabilities of the developmental system were somewhat disappointing but drastic improvements could be obtained in signal processing (reduce the noise bandwidth), increased transmission power, shot noise limited detector operation and the reduction of noise inserted in the filtering and mixing processing.

The alignment requirements of this type of system are extreme and would present problems in both fabrication and maintenance. Additionally, actual systems would have to be rigidly constructed and either environmentally controlled or fabricated with materials having nearly the same coefficient of thermal expansion.

B. RECOMMENDATIONS FOR FURTHER STUDY

There are several areas which warrant further study. One area would be to determine the exact mechanism causing the zero range frequency being imposed upon the local oscillator beam and determine the variation of this with different laser variables such as temperature and pressure broadening and different line operation.

Another and more intriguing question is that of the occurrence of the zero velocity frequency components in the velocity measurement part of the system investigation. Since all of the returned energy should have been doppler shifted in frequency, this presents a perplexing question.

It would also be worthwhile to extend the system development to determine the true limit of its capabilities. Initially this would require improvements in signal processing and perhaps eventually in the area of controls to develop steering and tracking capability.

Since a system operating at optical frequencies has such large doppler shifts for relatively low relative velocities, it may be feasible to determine the vibrational signatures of many objects (such as a jet engine of an aircraft) and utilize this in a target recognition scheme.

C. POSSIBLE SYSTEM APPLICATIONS

There are several possible applications for an optical radar. At the start of this project, it was hoped that clear air turbulence could be determined and that a lightweight low-power system could be developed for utilization in aircraft. There is still a possibility of this application being realized if system development is continued.

Another possible application is signature recognition as mentioned in the previous section. It is quite conceivable that a radar which could detect, provide range and velocity information and target identification could be developed along similar lines as this developmental system.

Another application which is both very desirable and conceivable would be in low flying, high closing speed target detection. The small beam size would allow detection of near the horizon targets with extremely fine bearing resolution capability. If a dual mode transmission capability were incorporated, a constant frequency beam could be transmitted and instant velocity determination of any return could be accomplished. If a doppler shift threshold were set (say for 400 knots relative speed) a threat warning system would be inherent. Upon recognition of a threat (and simultaneous velocity determination) the FM mode could be activated and range information provided.

The same characteristic which allows near the horizon search and high bearing resolution (small beam size) prevents the rapid scanning of a large volume of space. Thus any system for this threat recognition application would require numerous radars with each scanning a relatively small sector. With the advent of signal storage capability and digital processing and computer control, a system such as this may become feasible in the relatively near future.

APPENDIX A: EQUIPMENT LIST

Crystal Filter

Mfg. Damon	Model 6647A
f_o = 30 MHz	BW = 3.5 kHz

Optical Table

Mfg. UNIDEK
Stainless steel - honeycomb

CO_2 Laser

Mfg. Honeywell
Power 3 watt - vertically polarized

Amplifier (2)

Mfg. Hewlett Packard	Model 461A
Gain 20/40 db	Wideband

Oscilloscope

Mfg. Tektronix	Model 546

Signal Generator

Mfg. Wavetek	Model 134
Variable Frequency	Variable waveform

Signal Generator

Mfg. Hewlett Packard	Model 606A

Signal Generator

Mfg. Wavetek	Model 1001
Frequency sweeping	

Amplifier

Mfg. NELC	Bias-amp
Gain 23 db	NF - 3 db Wideband

Amplifier

Mfg. Miteo	Model Au-1A
Gain 30 db	NF - 5 db 2-100 MHz

Power Meter

Mfg. Coherent Radiation	Model 201

Power Meter

Mfg. Jodon	Model PM-550
< 200 mw	

Spectrum Analyzer

Mfg. Tektronix	Model 491

Power Supply (3)

Mfg. Hewlett Packard	Model 6216A
DC	

Frequency Counter

Mfg. CMC	Model 904

Balanced Mixers (2)

Mfg. Relcom	
.2 - 500 MHz	6 db insertion loss

Acousto-Optic Modulator

Mfg. Isomet	Model DE-IR-20
f_o - 40 MHz	BW - 10 MHz

Modulator Driver

Mfg. Isomet	Model DE-IR-10/5
f_o - 40 MHz	BW - 10 MHz
Power 0 - 5 w	

LIST OF REFERENCES

1. Skolnik, M. I., Radar Handbook, McGraw Hill, 1970.

2. Skolnik, M. I., Introduction to Radar Systems, McGraw Hill, 1962.

3. Bonnelle, G. J., "FM-CW Radar," Aerospace Electronics, p. 143-148, August 1960.

4. Hoisington, D. B., Multiple-Target CW FM Radar, paper presented at Asilomar Conference on Circuits and Systems, Sixth, Pacific Grove, California, November 1972.

5. Reference Data for Radio Engineers, 5th ed., P. Howard W. Sams & Co., New York, 1973.

6. Hymans, A. J., and Lait, J., "Analysis of a Frequency - Modulated Continuous-Wave Ranging System," Proceedings I.E.E.(British), p. 365-372, July 1960.

7. Richter, J. H., "High Resolution Tropospheric Radar Sounding," Radio Science, v. 4, no. 12, p. 1261-1268, December 1969.

8. Kay, L., "A Comparison Between Pulse and Frequency-Modulation Echo-Ranging Systems," Journal British I.R.E., p. 105-113, February 1959.

9. Yariv, A., Introduction to Optical Electronics, p. 305-333, Holt, Rinehart and Winston, 1971.

10. Adler, Robert, "Interaction Between Light and Sound," IEEE Spectrum, p. 42-54, May 1967.

11. Gordon, E. I., "A Review of Acousto-Optical Deflection and Modulation Devices," Proceedings IEEE, v. 54, no. 10, p. 1391-1401, October 1966.

12. Dixon, R. W. and Gordon, E. I., "Acoustic Light Modulators Using Optical Heterodyne Mixing," The Bell System Technical Journal, p. 367-389, February 1967.

13. Fang-Shang Chen, "Modulators for Optical Communications," Proceedings IEEE, v. 58, no. 10, p. 1440-1465, October 1970.

14. Pratt, W. K., Laser Communication Systems, Wiley, 1969.

15. Sze, S. M., Physics and Semiconductor Devices, p. 653-683, Wiley, 1969.

16. Oliver, B. M., "Thermal and Quantum Noise," Proceedings IEEE, p. 436-454, May 1965.

17. Hudson, R. D., Jr., Infrared System Engineering, Wiley, 1969.

18. Peyton, B., DiNarda, A., Chiou, W., Lange, R., Arams, F., Aita, M. and Pace, F., Coherent Infrared Receivers for Laser Communications and Radar, Internal paper of AIL, a division of Cutler-Hammer, Melville, Long Island, New York, 1973.

19. Rockwell International Science Center, 10.6 Micron Photodiodes, Miscellaneous Report, September 27, 1973.

20. Delange, O. E., "Optical Heterodyne Detection," IEEE Spectrum, p. 77-85, October 1968.

21. Mocker, H. W., "A 10.6 μm Optical Heterodyne Communication System," Applied Optics, v. 8, no. 3, p. 677-684, March 1969.

22. Isomet Corporation, Instruction Manual for 10.6 Micron Acousto-Optic Modulation System, December 1973.

23. Hogarth, C. A., Materials Used in Semiconductor Devices, Interscience Publishers.

24. Ross, M., Laser Receivers, Wiley, 1967.

25. Haliday, D. and Resnick, R., Physics Parts I & II, p. 1112, Wiley, 1966.

26. Read, W. S. and Fried, D. L., "Optical Heterodyning with Noncritical Angular Alignment," Proceedings IEEE, p. 1787, December 1963.

27. Fraunfelder, M. F., Jr., A Heterodyne Detection FM-CW Laser Radar Using a 10.6 μm Source, Engineers Thesis, Naval Postgraduate School, Monterey, California, December 1974.

INITIAL DISTRIBUTION LIST

		No. Copies
1.	Defense Documentation Center Cameron Station Alexandria, Virginia 22314	2
2.	Library, Code 0212 Naval Postgraduate School Monterey, California 93940	2
3.	Department Chairman, Code 52 Department of Electrical Engineering Naval Postgraduate School Monterey, California 93940	2
4.	Professor C. H. Rothauge, Code 52Rt Department of Electrical Engineering Naval Postgraduate School Monterey, California 93940	1
5.	Assoc Professor T. F. Tao, Code 52 Tv Department of Electrical Engineering Naval Postgraduate School Monterey, California 93940	1
6.	Asst Professor J. P. Powers, Code 52Po Department of Electrical Engineering Naval Postgraduate School Monterey, California 93940	1
7.	Dr. C. C. Wang (53/6241) Aeroject Electrosystems Co. 1100 W. Hollyvale Street Azusa, California 91702	1
8.	Dr. Greg Mooradian Code 2500 Naval Electronics Laboratory Center 271 Catalina Blvd. San Diego, California 92152	2
9.	Dr. J. Longo Rockwell International Science Center 1049 Camino Dos Rios Thousand Oaks, California 91360	1

10.	LT Maurice Fraunfelder, Jr. 1302 Putnam Avenue Janesville, Wisconsin 53545	1
11.	LT Thomas H. Chance, USN Naval Destroyer School Newport, Rhode Island 02840	1

20 APR 76
30 OCT 78
23501
25029

Thesis
C367
c.1

156335

Chance

FM-CW laser radar at 10.6 microns.

20 APR 76
30 OCT 78
23501
25029

156335

Thesis
C367
c.1

Chance

FM-CW laser radar at 10.6 microns.

thesC367
FM-CW laser radar at 10.6 microns.
3 2768 001 02365 8
DUDLEY KNOX LIBRARY